

MICROCOPY RESOLUTION TEST CHART
NATIONAL BUREAU OF STANDARDS-1963-A

2

NAVAL POSTGRADUATE SCHOOL

Monterey, California

AD-A155 163



DTIC
ELECTE
JUN 20 1985
B

THESIS

DTIC FILE COPY

DESIGN OF A GENERATOR FOR NEAR-TANGENTIAL
TRANSONIC SWIRLING OUTFLOW

by

Pamela E. Thrower-LeSesne

December 1984

Thesis Advisor: R. P. Shreeve

Approved for public release; distribution unlimited

85 6 3 056

Unclassified

SECURITY CLASSIFICATION OF THIS PAGE (When Data Entered)

REPORT DOCUMENTATION PAGE		READ INSTRUCTIONS BEFORE COMPLETING FORM
1. REPORT NUMBER	2. GOVT ACCESSION NO. AD-A155163	3. RECIPIENT'S CATALOG NUMBER
4. TITLE (and Subtitle) Design of a Generator for Near-Tangential Transonic Swirling Outflow		5. TYPE OF REPORT & PERIOD COVERED Master's Thesis December 1984
		6. PERFORMING ORG. REPORT NUMBER
7. AUTHOR(s) Pamela E. Thrower-LeSesne		8. CONTRACT OR GRANT NUMBER(s)
9. PERFORMING ORGANIZATION NAME AND ADDRESS Naval Postgraduate School Monterey, California 93943		10. PROGRAM ELEMENT, PROJECT, TASK AREA & WORK UNIT NUMBERS
11. CONTROLLING OFFICE NAME AND ADDRESS Naval Postgraduate School Monterey, California 93943		12. REPORT DATE December 1984
		13. NUMBER OF PAGES 117
14. MONITORING AGENCY NAME & ADDRESS (if different from Controlling Office)		15. SECURITY CLASS. (of this report) Unclassified
		15a. DECLASSIFICATION/DOWNGRADING SCHEDULE
16. DISTRIBUTION STATEMENT (of this Report) Approved for public release; distribution unlimited		
17. DISTRIBUTION STATEMENT (of the abstract entered in Block 20, if different from Report)		
18. SUPPLEMENTARY NOTES		
19. KEY WORDS (Continue on reverse side if necessary and identify by block number) Radial Outflow Vanes, Transonic Swirl Generation, Wedge-Arc Blading,		
20. ABSTRACT (Continue on reverse side if necessary and identify by block number) Two computer methods for the design of radial out-flow turning vanes are described. The key requirement was for vanes with simple shapes that could be machined easily and inexpensively in-house. Two design approaches, one using circular arcs for both suction and pressure sides and one for wedge-arc shaped sections were developed.		

DD FORM 1473
1 JAN 73

EDITION OF 1 NOV 65 IS OBSOLETE 1
S N 0102-LF-014-6601

Unclassified

SECURITY CLASSIFICATION OF THIS PAGE (When Data Entered)

Requirements for the general design procedure arose in two exploratory projects, a Rotary Detonative Wave Engine (RDWE) and a high speed Centrifugal Diffuser Test Device (CDTD). The RDWE was analyzed first and found to be potentially inefficient in its original configuration. Preliminary design for a high speed CDTD flow generator was completed, incorporating wedge-arc radial outflow vanes. An attempt to analyze the flow through the geometry using the Eidelman-Godnov Euler (EGE) was initiated.



Accession For	
NTIS CEASI	<input checked="" type="checkbox"/>
DTIC	<input type="checkbox"/>
Unannounced	<input type="checkbox"/>
Justification	
Distribution/	
Availability Codes	
Avail and/or	
Dist	
A-1	

Approved for public release; distribution unlimited

Design of a Generator for Near-Tangential
Transonic Swirling Outflow

by

Pamela E. Thrower-LeSesne
Lieutenant, United States Navy
B. S., University of California at Los Angeles, 1978

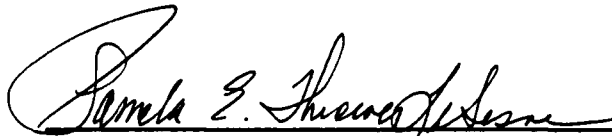
Submitted in partial fulfillment of the
requirements for the degree of

MASTER OF SCIENCE IN MECHANICAL ENGINEERING

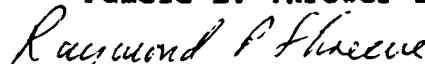
from the

NAVAL POSTGRADUATE SCHOOL
December 1984

Author:

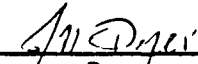

Pamela E. Thrower-LeSesne

Approved by:


Raymond P. Shreeve, Thesis Advisor


Robert H. Nunn, Second Reader


Paul J. Marto, Chairman,
Department of Mechanical Engineering


John N. Dyer, Dean of Science and Engineering

ABSTRACT

Two computer methods for the design of radial out-flow turning vanes are described. The key requirement was for vanes with simple shapes that could be machined easily and inexpensively in-house. Two design approaches, one using circular arcs for both suction and pressure sides and one for wedge-arc shaped sections were developed.

Requirements for the general design procedure arose in two exploratory projects, a Rotary Detonative Wave Engine (RDWE) and a high speed Centrifugal Diffuser Test Device (CDTD). The RDWE was analyzed first and found to be potentially inefficient in its original configuration. Preliminary design for a high speed CDTD flow generator was completed, incorporating wedge-arc radial outflow vanes. An attempt to analyze the flow through the geometry using the Eidelman-Godnov Euler (EGE) was initiated.

Design Requirements Document: 10/19/75

TABLE OF CONTENTS

I. INTRODUCTION----- 13

II. APPARATUS DESIGN----- 17

 A. DESIGN CONSIDERATIONS----- 17

 B. APPARATUS DESCRIPTION----- 18

 C. DESIGN CALCULATIONS----- 19

III. BLADING DESIGN----- 22

 A. BACKGROUND----- 22

 B. DESIGN METHOD----- 23

IV. FLOW ANALYSIS----- 25

 A. METHODS----- 25

 B. RESULTS----- 27

V. SUMMARY AND DISCUSSION----- 29

VI. CONCLUSIONS AND RECOMMENDATIONS----- 34

 A. CONCLUSIONS----- 34

 B. RECOMMENDATIONS----- 35

APPENDIX A TORQUE PRODUCED BY DISTRIBUTED
GAS REACTION----- 49

 A.1 METHODS----- 49

 A.2 RESULTS----- 54

APPENDIX B DOUBLE CIRCULAR ARC BLADING DESIGN----- 59

 B.1 METHOD----- 59

 B.2 COMPUTER PROGRAM "ACIRC"----- 70

 B.2.1 Description----- 70

B.2.2 Required Inputs-----	71
B.2.3 Listed Outputs-----	71
B.2.4 Program Listing-----	73
APPENDIX C WEDGE ARC BLADING DESIGN-----	87
C.1 METHOD AND MODIFICATIONS-----	87
C.2 COMPUTER PROGRAM "AWEDG"-----	95
C.2.1 Description-----	95
C.2.2 Required Inputs-----	96
C.2.3 Listed Outputs-----	97
C.2.4 Program Listing-----	98
LIST OF REFERENCES-----	114
BIBLIOGRAPHY-----	116
INITIAL DISTRIBUTION LIST-----	117

LIST OF TABLES

1.	Required Design Dimensions for Convergent Throat in High Speed CDTD-----	36
2.	First Order Solution of Euler Equations-----	37
A1.	Specific Power and Power Conversion Efficiency Vs Velocity Ratio Data-----	58
B1.	List of Computer and Text Symbols for Double Circular Arc Blades-----	77
C1.	List of Computer and Text Symbols for Wedge Shaped Arc Blades-----	103

LIST OF FIGURES

II.1 Description of Conditions at Throat-----	20
II.2 Cross Sectional View of the Test Section-----	21
1. Schematic of Detonation Rotor Concept-----	38
2. Schematic of the Low Speed CDTD-----	39
3. Schematic of the Proposed High Speed CDTD.-----	40
4. CDTD Flow Generator Section AA	
from Figure 3-----	41
5. Two-Dimensional Turbine Cascade-----	42
6. Axial Turbine Blade Geometrical Design-----	43
7. Final Blading Design-----	44
8. Computational Grid and Boundary	
of the Comutational Domain-----	45
9. Computational Grid Notation-----	46
a) Grid Location in Coordinate System-----	46
b) Single Cell-----	46
10. Computational Grid for Outflow Analysis-----	47
11. Enlargement of the Grid in the	
Throat Region-----	48
A1. Velocity Triangle of Conventional	
Cylindrical Flow-----	51
A2. Velocity Diagram at Exit of Rim-----	51
A3. RDWE Specific Power Vs. Velocity Ratio-----	55

A4.	RDWE Power Conversion Efficiency	
	Va. Velocity Ratio-----	56
B1.	Double Circular Arc Blade	
	Geometrical Description-----	80
B2.	Geometrical Description for	
	Camber Line Tangency Condition-----	81
B3.	Continued Geometrical Description	
	for Camber Line Tangency Condition-----	82
B4.	Function of ψ Resulting from the Condition of	
	Tangency of the Camber Line (equation B(50))-----	83
B5.	Schematic for Rotation of Axes-----	84
B6.	Computer Generated Shapes for a 60	
	Blade Design-----	85
B7.	Computer Generated Blade	
	Passage for a 60 Blade Design-----	86
C1.	Relaxed Double Circular Arc Passage	
	with Pressure Line Removed-----	108
C2.	Wedge Arc Shaped Blading Geometry-----	109
C3.	Enlarged View of Trailing Edge-----	110
C4.	Geometrical Relationship Between	
	Throat Dimension and Suction Surface Radius-----	111
C5.	Computer Generated Shapes for a Cascade of	
	Wedge Arc Shaped Blades with 60 Blades-----	112
C6.	Computer Generated Blade Passage	
	for Wedge-Arc Shaped Blades-----	113

NOMENCLATURE

A^*	throat area
A_h	throat area for High Speed CDTD
A_l	throat area for Low Speed CDTD
a	throat dimension
b	width test section
D	outer diameter
e	energy of the unit volume
L	length of blades
\dot{m}	mass flow rate
P	power
P_s	specific power
p	pressure
R	radius of curvature
r_1	inner radius
r_2	outer radius
s	blade spacing
T	torque
U	velocity component corresponding to x coordinate
U_n	velocity component normal to edge
U_2	wheel rim velocity
V	velocity component corresponding to y coordinate
V_t	velocity component tangent to edge

$V_{\theta 1}$ tangential component of inlet velocity
 $V_{\theta 2}$ tangential component of outlet velocity
 W_2 relative exit velocity
 W_x work
 w' rotational velocity
 Z number of blades
 α efflux angle
 β_2 blade exit angle with respect to radial direction
 β_2' negative blade exit angle with respect to radial
direction
 τ specific heat ratio
 ϵ internal energy
 η_c power conversion efficiency
 ρ density

Notations used in Appendices B and C are independently
defined therein.

IV. FLOW ANALYSIS

A. METHOD

A FORTRAN computer program for solving numerically the two-dimensional Euler equations using the Godunov method was developed at the Turbopropulsion Laboratory by Dr. S. Eidelman [Ref. 12]. With Dr. Eidelman's help the program was to be applied to obtain a prediction of the flowfield through the vane passage. An abbreviated description will be given here of the computational method.

The unsteady two-dimensional Euler equations are written as

$$\frac{\partial \underline{a}}{\partial t} + \frac{\partial \underline{b}}{\partial x} + \frac{\partial \underline{c}}{\partial y} = 0 \quad (7)$$

where

$$\underline{a} = \begin{vmatrix} \rho \\ U \\ V \\ e \end{vmatrix}, \quad \underline{b} = \begin{vmatrix} \rho U \\ p + \rho U^2 \\ UV \\ (e+p)U \end{vmatrix}, \quad \underline{c} = \begin{vmatrix} \rho U \\ \rho UV \\ p + \rho V^2 \\ (e+p)V \end{vmatrix}$$

and

$e = \rho (\epsilon + (U^2 + V^2)/2) = \text{energy of a unit of volume}$

$\epsilon = \frac{p}{(\gamma - 1)\rho} = \text{internal energy}$

$\rho = \text{density}$

U and V are the velocity components corresponding to the x and y coordinates

$p = \text{pressure}$

$\gamma = \text{specific heat ratio.}$

Modifications were made to the double circular arc design to achieve convergency at the exit. The first step was to remove the pressure line and use the camber line as the pressure surface. The assumption was made that the effects associated with inlet flow incidence resulting from the removal of the pressure line would be negligible. The results indicated that the passage was indeed converging toward the exit. The second step in an attempt to assure tangency and convergency at the exit was to allow for a thickness and a straight section at the leading and trailing edges. The straight section was such that a specified throat dimension was achieved at the trailing edge of the adjacent previous vane. The resulting program, which is presented in Appendix C, designs a wedge shaped arc blade such that a passage which converges at the exit is realized with a specified throat dimension. Using the method a high speed CDTD blading design was obtained. Figure 7 shows the resulting blade design.

literature [Ref. 8,9,10,11, and 12 for example]. Yet none was found which dealt with the required case of radial-outflow.

B. DESIGN METHOD

The expansion process in a radial turbine differs appreciably from that in an axial turbine because of the radius changes. Vavra's work [Ref. 5] involved axial turbine design. The work presented here for radial-outflow vane design followed an appreciation of Vavra's methods and possibly retraced steps of others who have previously sought the simplest geometries for machining purposes.

The simplest shape, that of double circular arcs was attempted first. Its development is presented in Appendix B. It was anticipated that with the requirements of radial inlet flow and tangential exit outflow the double circular arc method could be used in the design of radial-outflow turning vanes. Once the method was developed and exercised it was clear that more geometrical constraints were required to produce a nozzle with an exit which was both nearly-tangential and convergent.

The double circular arc program generated vanes which appeared to converge within the passage and then diverge towards the exit of the nozzle. Therefore, the flow would choke within the nozzle and the outlet flow conditions could not be predicted very well.

III. BLADING DESIGN

A. BACKGROUND

In Ref. 5 Vavra gave a procedure to establish a blade profile for specified values of throat width a , spacing s , trailing edge thickness t_e , and inlet flow angle, α . Figure 6 illustrates these features.

Vavra's design was for axial turbine blades or vanes. A computer program was available to construct blading following Vavra's methods [Ref. 5]. The method used circular arcs, and straight lines. Wedge angles and leading and trailing edge radii were input parameters to determine a flow channel with suitable acceleration. No comparable method and program were found for radial outflow vanes.

In 1968 Goldman and Scullin [Ref. 8] designed blades with inlet transition arcs, circular arcs and outlet transition arcs. However, these blades were not converging at the exit and were not designed for radial-outflow.

Later Goldman and Vanco [Ref. 9] developed a computer program for the design of sharpened-edged throat supersonic nozzles for isentropic flow. Their program was constructed for the radial-inflow case. The Goldman and Vanco design also involved the requirement of contour machining.

There is a substantial amount of information on both radial-inflow and axial turbine blade design in the

$$(A^*/A_1)^{1/2} = (6.27/38.5)^{1/2} \approx .40. \quad (5)$$

Using this scale factor, the dimensions calculated for the high speed model are shown in the following sketch.

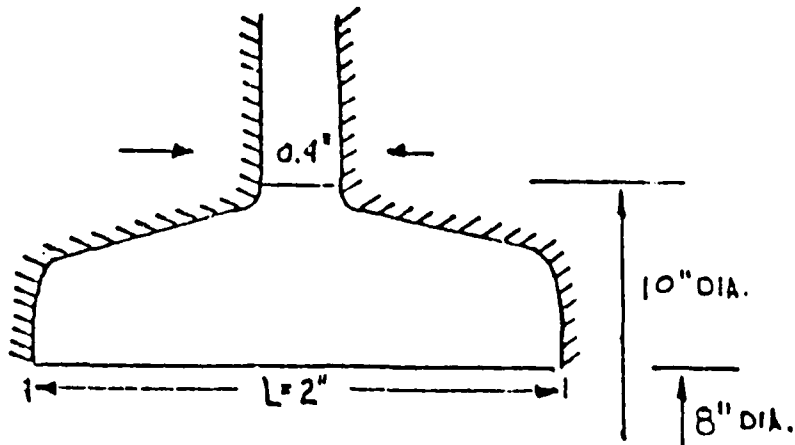


Figure II.2 Cross Sectional View of the Test Section

From equations (2),

$$a z = A^* / L \quad (6)$$

therefore for a diameter of 8 inches we can predict a required throat dimension, and blade spacing using equation (3) for a selected number of blades. Results are given in table 1. The requirement then is to design suitable turning vanes to produce the required throat area and spacing.

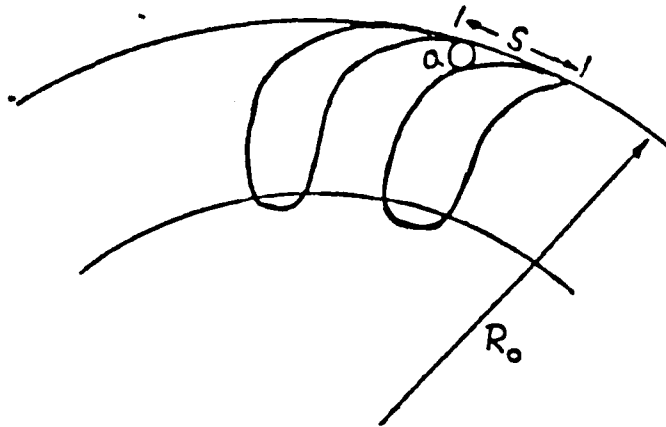


Figure II.1 Description of Conditions at Throat

The blade spacing, s , is given by

$$s = \pi D / Z \quad (3)$$

where D is the diameter at the vane exit. From equations (2) and (3),

$$A^* = L (a/s) \pi D. \quad (4)$$

In Ref. 7, the following conditions were calculated for a "full scale" high speed CDTD design to have a test section width of 1 inch at 25 inches diameter:

$M_1=1.5$ at $\beta_1=55^\circ$, at $R_1=12.5$ inches
 $V_1=1392$ ft/sec at $T_0=520$ °R, giving
 $V\theta_1=1140$ ft/sec and $V_{R_0}=1357$ ft/sec and for
 a swirl vane length of 5 inches, $V_{R_0}=182$ ft/sec
 and $\beta_0=82.34^\circ$. An increase of swirl vane length
 to 5.713 inches gave $V_{R_0}=160$ ft/sec and $\beta_0=83.3^\circ$

Using the above data for the "full scale" high speed CDTD in equation (4), $A^* = 38.5$ inches². Using a linear scaling to the model in which $A^* = 6.27$ inches², the scale factor is

C. DESIGN CALCULATIONS

Vavra [Ref. 5] showed that in the design of a turbine cascade the efflux angle α can be calculated from the geometry of the cascade and that it is independent of the incidence angle i of the inlet velocity, see Figure 5. Vavra also noted that it is common practice in steam turbine design to use the relation

$$\alpha = \arccos (a / s) \quad (1)$$

where "a" is the throat opening at the discharge and s is the blade spacing. Equation (1) applies when the trailing edges of the blades are of negligible thickness. In practice the "wedge" angle at the trailing edge and trailing edge bluntness modifies this dependence.

With the limitation of a two minute runtime and the available mass of stored air, Demo [Ref. 6] found that for the supersonic cascade rig in building 230 an area of 6.27 square inches was needed at the nozzle throat where the flow would choke. This same area was taken for the total outlet throat area of the swirl vanes for the high speed CDTD.

Referring to the following sketch, the area at the exit where the flow will choke, A^* , is given by,

$$A^* = L a Z \quad (2)$$

where L is the vane length, a is the throat width and Z is the number of vanes.

required across the swirl generator in the high speed version, turbine like turning vanes were selected rather than the sheet metal nozzle construction used in the low speed device.

B. APPARATUS DESCRIPTION

Figure 3 illustrates the overall arrangement of the proposed CDTD design. The swirl vanes for the high speed CDTD are sandwiched between two circular plexiglas disks. Plexiglas disks were used to allow visualization of the flow through the vanes. The disks are mounted on an aluminum center pipe shown in Figure 3. The pipe provides double axial in-flow. Following the work performed by Feieresien [Ref. 4] a transition section to turn the air from the axial to the radial direction was added in the form of a plate on a tie-rod on the pipe centerline. The design of the transition section is not complex if the area of the radial outlet is smaller than that of the total axial inlet. An acceleration through the transition section will then occur, leading to generally favorable pressure gradients. These considerations required a double-entry supply arrangement for the CDTD model.

The piping is attached to the air supply system. Figure 4 shows the configuration of the blades on the plexiglas disks and in relationship to the supply pipe.

II. APPARATUS DESIGN

Factors considered in the design of the high speed CDTD fell into two categories; namely, limitations due to the available air supply system and piping and the requirement that the test section have dimensions appropriately scaled for the diffusers required to be tested.

A. DESIGN CONSIDERATIONS

The high speed CDTD was designed to operate as an intermittent blow-down wind tunnel. In order to use the air supply system available in building 230 at the Naval Postgraduate School, the test section flow area was dictated by the available mass of stored air and the minimum desired runtime of two minutes. Using proportions similar to those used in the low speed CDTD (see Figure 2), the radius of the swirl generator became four inches while the radius at the test section was five inches. The method used for calculating these dimensions is given in the following section. The difference between the swirl generator outer radius and the test section radius allowed for mixing of the wakes from the blading (or nozzles) used in the swirl generator. The swirl generator was limited to a length of two inches to meet the scaling requirements set by the test section. Because of the larger pressure differential

apparatus are described. General methods and computer programs for the design of double circular arc and wedge arc blading for radial-outflow vanes are described in detail in appendices. The report also discusses a method of predicting the flowfield through a selected passage using an Euler code based on the Godunov method of solution.

development for viscous, three dimensional, transonic flow (a regime containing both supersonic and subsonic regions), with adverse static pressure gradients. Such methods are required to design optimum radial diffusers for transonic conditions. Equally, a high speed version of the CDTD was required in order to examine such diffuser flows under controlled conditions and to verify the emerging codes. Again, nearly tangential swirling outflow was required, this time in steady flow.

The main interest here was therefore to design vane shapes and the apparatus for a high speed CDTD. The design would closely parallel the general arrangement of the low speed CDTD. The high speed CDTD, had the unusual requirement of radial-outflow with convergency at the rim exit. The limitation on the design was primarily that the hardware could be machined easily and inexpensively in-house. Computer programs for the design of supersonic nozzles for radial-inflow turbomachines were found to exist, but most were highly involved and would need extensive machining processes to generate the blade shapes. Particular designs are discussed herein. A literature search indicated that computer programs for radial-outflow devices using simple vanes for two-dimensional isentropic flow of a perfect gas were not available.

In the present report, the design of the blading for a high speed CDTD model and the general arrangement of the

The question then was, what would be the best design for the rotor passage to maximize the torque impulse? In an analysis included in Appendix A it was shown that tangential flow at the rim of the RDWE would yield the highest specific power and highest power conversion efficiency. A design was required therefore of nozzles which would direct the outflow almost tangentially. The nozzles would operate in an unsteady mode.

The second project which motivated the present study involved the development of a test rig for radial diffusers. Such diffusers are used in centrifugal compressors to convert the kinetic energy of the flow from the rotor into static pressure. Erwin [Ref. 2] proposed and designed a so-called low speed Centrifugal Diffuser Test Device, (CTD). The CTD simulated the flow of air delivered to the diffuser from the compressor rotor using static swirling vanes. The facility would allow the evaluation of proposed new diffuser geometries and permit validation of computer analyses for diffusers operating in the fully subsonic flow regime. Figure 2 shows a schematic of the low speed CTD. Vidos [Ref. 3] presented results from the flow generator used in the CTD and performed an analysis of the internal flow. As mentioned by Vidos, the design of centrifugal diffusers is presently based on experimental results for two dimensional and conical diffusers. Numerical methods are currently under

I. INTRODUCTION

The motivation for the work reported here came from two exploratory projects, a Rotary Detonative Wave Engine, (RDWE), described in Ref. 1 and a high speed Centrifugal Diffuser Test Device (CDTD), described in Ref. 2. Both projects required the geometrical design of an axisymmetric generator for nearly-tangential transonic outflow.

To improve gas turbine engine performance an increase in cycle pressure ratio is needed. One alternative to mechanical compression is to supply the compression thermally by detonative combustion. If the pressure rise produced in this manner is sufficient for the engine, no compressor and associated drive turbine are required and a simpler more efficient engine might result.

As described by Monks [Ref. 1] , a proposed geometry for such an engine might include a rotor with outflow passages which are turned at the exit to produce nearly tangential flow. Figure 1 illustrates the proposed RDWE. Monks attempted to measure the torque on a static simulated rotor as a detonation wave propagated from the center outward. A reaction torque was produced from the nearly-tangential expulsion of gases from the rim.

ACKNOWLEDGEMENT

Work in support of the development of a transonic "Centrifugal Diffuser Test Device" by the U.S. Army's Propulsion Laboratory, at the NASA Lewis Research Center, provided in large part the motivation for the work presented here.

Equation (7) is nondimensionalized using arbitrary reference quantities, and the Godunov method [Ref. 12] is applied to compute at each time interval the fluxes at the boundaries of the cells of a grid established for the problem under consideration. The steady state solution is found when no further change occurs between successive time steps.

The computational domain is shown for a typical cascade problem in Figure 8 and the grid and cell notation are defined in Figure 9. Referring to Figure 8, for the tangency condition at the wall of the passage a solid wall boundary condition is imposed over the segments 3-5 and 4-5. Boundary conditions for segments 1-3, 5-7, 2-4 and 6-8 are for periodicity of the flow with respect to the y axis.

The parameters held constant at the inlet are the x components of velocity, U , the flow angle, θ , the gas stagnation enthalpy, H , and the entropy, S . The velocity, density and pressure can be calculated from these quantities easily as V_{in} , ρ_{in} , and p_{in} . At the outlet boundary only pressure is defined and other flow parameters are calculated in the solution. In the solution procedure, U_{out} , V_{out} , and ρ_{out} are set equal to the values of U , V and ρ one point ahead of the outlet boundary.

A subroutine (program) constructs a non-orthogonal grid covering the computational domain as shown in Figure 9. The flow parameters related to the center of the cell have a

fractional index: $j+\frac{1}{2}$, $k+\frac{1}{2}$. The cell boundaries have one fractional and one integer index: j , $k+\frac{1}{2}$ or $m+\frac{1}{2}$, n . The parameters at the time t will have subscript indices and at time $t+\delta t$ the parameters will have superscript indices.

The Euler equation is approximated to first order by the equation in table 2. Solution to the Riemann problem is initiated assuming that the left state is that located at $j-\frac{1}{2}, k+\frac{1}{2}$ and the right state is that at $j+\frac{1}{2}, k+\frac{1}{2}$.

The solution to the Riemann problem will give

$$(R, P, U_n, V_t)_{j, k+\frac{1}{2}}$$

U_n = the velocity component normal to
the edge $(j, k+1) - (j, k)$

V_t = the velocity component tangent to
the edge $(j, k+1) - (j, k)$

The capital letters R (rho), U , V , P are the parameters calculated at the edges of the zones.

The component of the velocity is then transformed back to the cartesian coordinate system and a final value of the parameter on the cell edge is received

$$(R, P, U_n, B)_{j, k+\frac{1}{2}}$$

B. RESULTS

The program (EGE) was run on the IBM 370-3033 at the Naval Postgraduate School. Figure 10 illustrates the grid covering the passage for the wedge-arc blading shown in

Figure 7. An enlargement of the exit area is shown in Figure 11.

In order to apply the code to the radial geometry, some modifications were necessary. A transformation of coordinates was made to conveniently accommodate the radial flow inlet boundary condition. Since the program remained basically two-dimensional, the outlet flow was treated as being periodic over the blade space at the exit which then did not change with radius. Thus the solution found will be valid for the flow within the rim and approximately true just outside the rim. For this reason the computational domain in Figure 11 was not extended radially outwards beyond one blade space.

Results could not be obtained for the flow through the passage within the time available. Some difficulties were encountered by the program in the region of the throat. Some modifications of the grid must be made before a converged, steady flow solution can be obtained.

V. SUMMARY AND DISCUSSION

Two exploratory projects at the Turbopropulsion Laboratory, 1). to test the concept of detonative combustion as an alternative to mechanical compression in gas turbines and 2). to design a test rig for radial diffusers used in centrifugal compressors, were examined. The projects were similar in nature since they involved the generation of nearly-tangential radial outflow and each required a design of turning vanes for a test apparatus. The overriding limitation for either project was that any apparatus developed would have to be easily and inexpensively manufactured in-house.

In the Rotary Detonative Wave Engine, "RDWE", project, turning vanes were required such that upon detonation the maximum possible torque impulse would be obtained. The best design possible to yield maximum power hence maximum torque was to produce turning vanes that exit nearly-tangential. Using Euler's Turbine equation a relationship was developed relating exit angle to specific power and efficiency.

The results for the unsteady expansion process showed that the value of the relative flow angle (β_2) established the limiting conversion efficiency and specific power. If the relative velocity increases beyond the limiting point the specific power generated will be absorbed rather than generated and efficiency will decrease. High efficiency

occurs in large part only when the specific power is low or at the limiting point. In general the conversion efficiency will vary during the expansion process, but will always be poor.

This result implies that the concept of the RDWE can not be efficient as a stand alone rotor. Other methods would have to be employed to increase efficiency, such as the utilization of additional components, particularly those which would allow nearly constant flow by sequencing the detonation wave with respect to partial ports.

The second project involved the development of a test rig for a high speed Centrifugal Diffuser Test Device, "CDTD". The project would closely parallel an in-house concept of a low speed CDTD. The low speed version simulates the flow of air delivered to a diffuser as a steady process. The high speed version simulates in a steady process, the transonic Mach numbers characteristic of advanced centrifugal compressors.

For the high speed CDTD a passage would be required which would cause the flow to converge and choke at the exit of the passage. Because the concept of the RDWE was questionable the main interest turned to designing vane shapes and the apparatus for a high speed CDTD.

Two methods and their respective computer programs were developed. The first method involved the development of double circular arc vane shapes. Given the outer radius, the inner radius and the number of blades the radii of the suction

and pressure sides were determined. The design emphasis was on achieving a tangent suction surface at the exit and a radial camber line at the inner radius. The concurrent condition of a tangent camber line at the exit gave the solution of a blade of zero thickness.

The geometrical description resulting in a tangent camber line at the exit, resulted in the sine of the camber angle ϕ being equal to the cosine of the subtended blade angle γ . Following manipulations to relate the value of γ to just the radius ratio (the only specified parameter), an equation of fourth order in $\sin \gamma$ resulted. Using Newton's method of iteration the first (smaller) root was found. Using this value of γ a blade shape was generated. It was clear that the suction side was tangent but the efflux angle α was not zero. An efflux angle of zero would indicate that the camber line was also tangent to rim. A graph of the fourth order function indicated that two roots were possible for each radius ratio. Only the first root was solved for. It is probable that the second root would yield the tangency condition of both camber line and suction side. The selected root was shown however to give $\sin \phi = \cos \gamma$.

It was realized that convergence at the exit could not be guaranteed with the double circular arc blade design. Modifications were applied to the design to cause the passage to converge. Improved convergence resulted when the original camber line and the suction line were used to describe the

blade. The simple double circular arc design required curved or thin trailing edges. With the addition of a finite thickness at the leading and trailing edge, a straight line segment, and a wedge angle all of which would better direct the flow in the tangent direction, practical blade shapes with convergent passage were achieved.

Geometrical equations were developed to yield the proper blade design. The exit throat dimension was fixed in the design based on the limitations of the available air supply and based on dimensions scaled from a high speed CDTD design. It was anticipated that the flow would choke at the specified throat dimension between adjacent suction and pressure sides and the straight line segment would intersect the exit circle which was tangent to the suction side. This did not occur. The length of the straight line segment varied between 1 and 5 percent of the value needed for this condition. It was not required that the exit circle be tangent to the pressure side.

From the geometry and the specified parameters a blade was developed giving convergency at the exit. The camber angle θ and the subtended blade angle γ were specified from experience obtained in the development of the double circular arc design. The chosen angles θ and γ gave an efflux angle α between 8 and 9 degrees. To achieve the perfect condition of tangential flow angle α would be required to be equal to zero. Based on current technology and manufacturing abilities an angle in the area of 8 or 9 degrees would give as close to

tangential flow as is possible. It is noted that the angle ϕ is related uniquely to the angle ψ . Once the radius ratio is given.

The coordinates of the designed passage were then input into the FORTRAN program (EGE) to predict analytically the flowfield through the vane passage, by solving the Euler equations. The program (EGE) was designed to run on the IBM 370-3033. The program successfully constructed a non-orthogonal grid covering the domain, however results could not be obtained for the flowfield through the passage in the initial attempts. It is thought that the difficulty lies in the curvature and density of the grid in the region of the exit throat. Since the EGE program has not previously been applied to a radial outflow problem with severe curvatures the task of analyzing the present flow with the EGE code is now thought to require the concentrated effort of the code's author.

In contrast, the CDTD vane design can be manufactured without difficulty and the flow from the turning vanes can be measured experimentally. It is suggested that such an experiment would provide a severe test of the ability of the EGE code to simulate transonic radial outflow containing embedded waves.

VI. CONCLUSIONS AND RECOMMENDATIONS

A. CONCLUSIONS

The following conclusions are offered:

The Rotary Detonation Wave Energy concept in its original configuration is potentially inefficient. An increase in efficiency would require the addition of a component which could recover the unsteady kinetic energy of the flow leaving the rotor.

A program for designing radial outflow vanes using double circular arc blades was demonstrated successfully. While the method may be useful in other contexts, it was found to be unable to produce converging passage shapes with a near-tangential outlet flow direction.

A program for designing radial outflow vanes using wedge-arc blade shapes was used successfully to produce converging passage shapes with prescribed throat widths and with a near-tangential outlet flow direction.

Both blade shapes can be produced relatively inexpensively from standard metal stock.

A preliminary design of a test model of a high speed Centrifugal Diffuser Test Device was produced.

B. RECOMMENDATIONS

The following recommendations and areas of further investigations are suggested:

An arrangement of partial porting and following power turbine for the Rotary Detonation Wave Engine should be examined.

The program for double circular arc blades should be modified to seek both roots of the condition for camber line tangency, and to offer the selection of any value of ψ between them. This will result in the ability to examine any value of ψ within the range of any practical interest.

In the case of wedge-arc blades, the possibility of solving for the particular case in which the circle at the passage outlet is also tangent to the pressure side should be examined. A procedure should also be introduced to calculate the progression of the passage area taking into account the increasing radius.

The proposed blading geometry should be constructed and the outlet flowfield examined experimently.

Work should be continued to obtain a computational prediction of the flow through the passage. The model test could then serve as a verification of the code.

TABLE 1. Required Design Dimensions for Convergent Throat in High Speed CDTD.

NUMBER OF BLADES	THROAT DIMENSION	SPACING
2	a (in.)	s (in.)
6	.5225	4.1888
12	.2613	2.0944
18	.1742	1.3963
36	.08708	.6981
45	.06967	.5585
60	.05225	.4189

TABLE 2. First Order Solution of Euler Equations

$$\bar{a}_{j+\frac{1}{2},k+\frac{1}{2}} = \bar{a}_{j+\frac{1}{2},k+\frac{1}{2}} - \frac{\Delta t}{j+\frac{1}{2},k+\frac{1}{2}} \cdot$$

$$(B_{j+\frac{1}{2},k} \cdot \Delta Y_{j+\frac{1}{2},k} - C_{j+\frac{1}{2},k} \cdot \Delta X_{j+\frac{1}{2},k} +$$

$$B_{j+\frac{1}{2},k+\frac{1}{2}} \cdot \Delta Y_{j+\frac{1}{2},k+\frac{1}{2}} - C_{j+\frac{1}{2},k+\frac{1}{2}} \cdot \Delta X_{j+\frac{1}{2},k+\frac{1}{2}} +$$

$$C_{j+\frac{1}{2},k+1} \cdot \Delta X_{j+\frac{1}{2},k+1} - B_{j+\frac{1}{2},k+1} \cdot \Delta Y_{j+\frac{1}{2},k+1} +$$

$$C_{j,k+\frac{1}{2}} \cdot \Delta X_{j,k+\frac{1}{2}} - B_{j,k+\frac{1}{2}} \cdot \Delta Y_{j,k+\frac{1}{2}})$$

where

$$\sigma_{j+\frac{1}{2},k+\frac{1}{2}} = \frac{1}{2} (X_{j+1,k+1} - X_{j,k}) (Y_{j,k+1} - Y_{j+1,k}) -$$

$$(X_{j,k+1} - X_{j+1,k}) (Y_{j+1,k+1} - Y_{j,k})$$

$$\Delta Y_{j,k+\frac{1}{2}} = Y_{j,k+1} - Y_{j,k}$$

$$\Delta X_{j+\frac{1}{2},k} = X_{j+1,k} - X_{j,k}$$

$$\bar{a} = \begin{vmatrix} \rho \\ \rho U \\ \rho V \\ e \end{vmatrix}, \quad \bar{B} = \begin{vmatrix} RU \\ P+RU^2 \\ RUV \\ (E+P)U \end{vmatrix}, \quad \bar{C} = \begin{vmatrix} RU \\ RUV \\ P+RV^2 \\ (E+P)V \end{vmatrix}$$

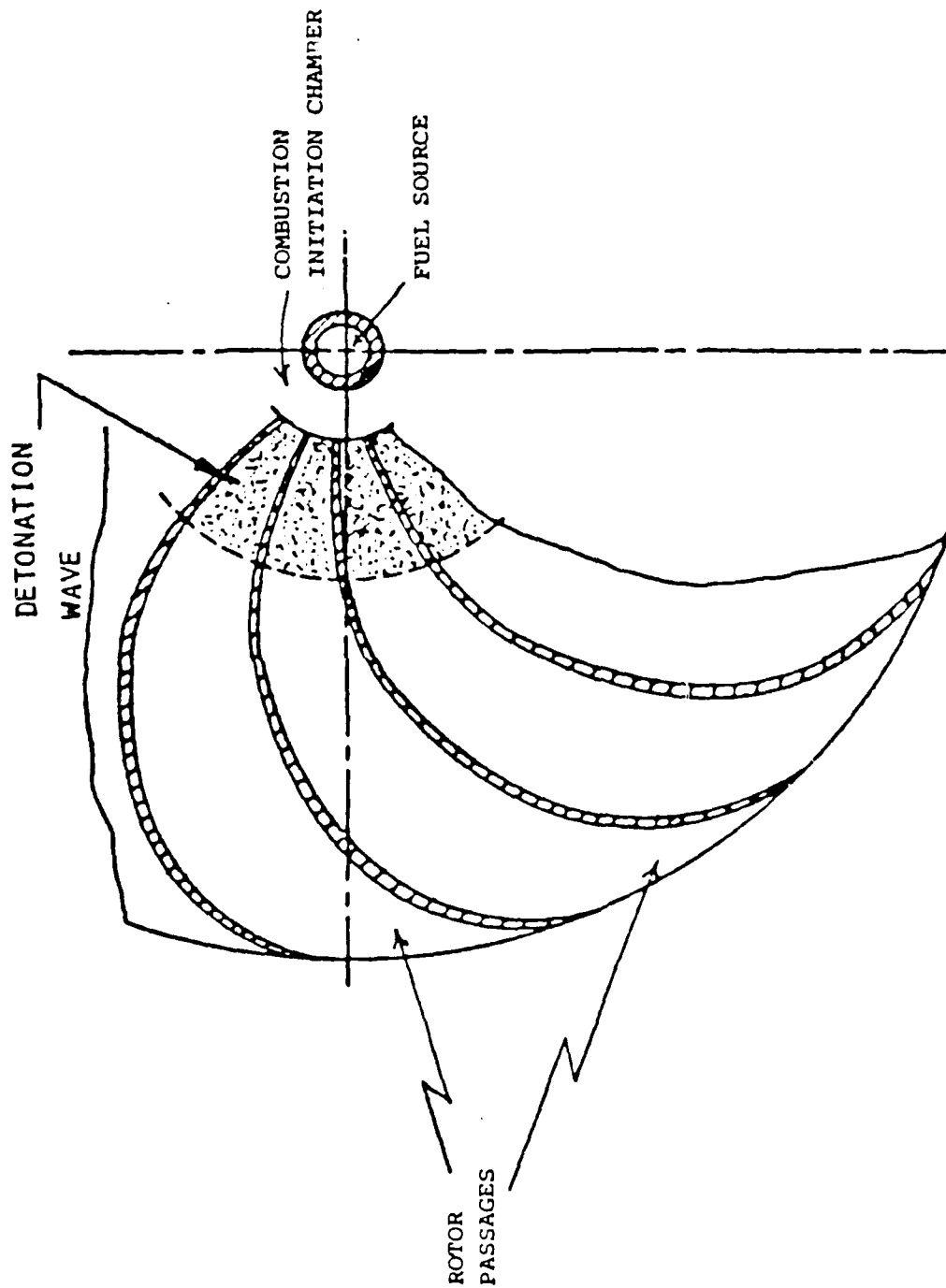


Figure 1. Schematic of Detonation Rotor Concept.

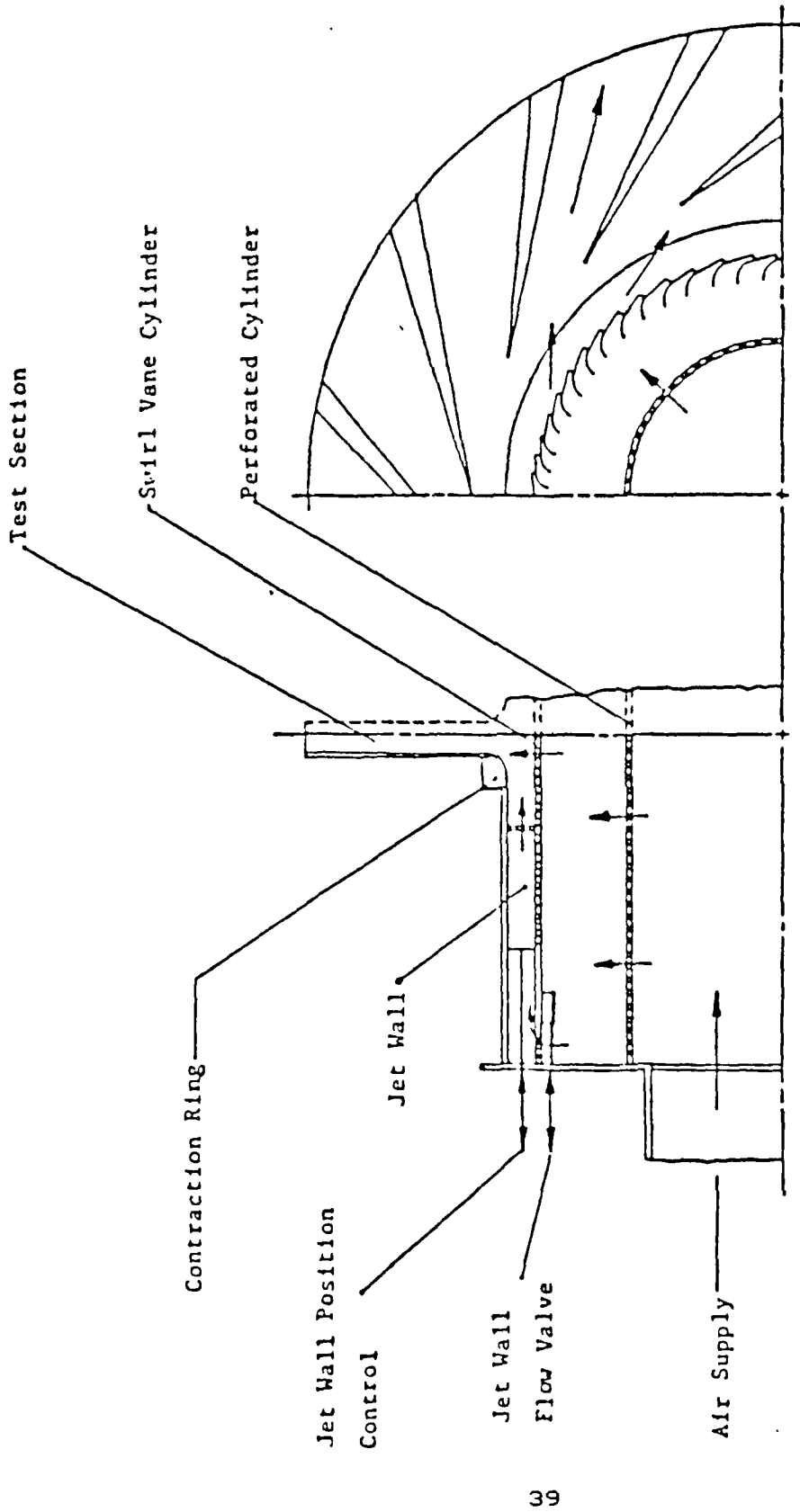


Figure 2. Schematic of the Low Speed CTD.

$$\frac{1}{2}V^2 = \frac{1}{2}U_2^2 \left[-\frac{2W_2}{U_2} \sin \beta_2' + 1 + \frac{W_2^2}{U_2^2} \right] \quad A(13)$$

Substituting equation A(10) and A(13) into A(9)

$$\begin{aligned} \eta_c &= \frac{P/\dot{m}}{P/\dot{m} + \frac{1}{2}V^2} \\ &= \frac{U_2^2 \left(\frac{W_2}{U_2} \right) \sin \beta_2' - 11}{U_2^2 \left[\left(\frac{W_2}{U_2} \right) \sin \beta_2' - 1 \right] + \frac{1}{2}U_2^2 \left[-\frac{2W_2 \sin \beta_2' + 1 + \frac{W_2^2}{U_2^2}}{U_2} \right]} \\ &= \frac{\left(\frac{W_2}{U_2} \right) \sin \beta_2' - 1}{-\frac{1}{2} + \frac{1}{2} \left(\frac{W_2^2}{U_2^2} \right)} \end{aligned}$$

$$\eta_c = -\frac{2 \left[\left(\frac{W_2}{U_2} \right) \sin \beta_2' - 1 \right]}{\left(1 - \frac{W_2^2}{U_2^2} \right)} \quad A(14)$$

Equations A(10) and A(14) are valid for a discrete jet, or for distributed gas at the rim. For the distributed gas, it is possible to calculate the referred power as a function of wheel radius, giving specific power, P_s . Using equation A(10),

$$P_s = P/\dot{m}U_2 = \left[\left(\frac{W_2}{U_2} \right) \sin \beta_2' - 1 \right] \quad A(15)$$

Therefore equation A(14) becomes,

$$\eta_c = \frac{2 P_s}{\left(\frac{W_2}{U_2} \right)^2 - 1}$$

For $\sin \beta_2' = 1$, implying that $\beta_2' = 90$ degrees,

$$\eta_c = \frac{2}{\left(\frac{W_2}{U_2} \right) + 1}$$

therefore

$$V\theta = W \sin \beta + U \quad A(7)$$

Substituting equations A(7) into A(5) we obtain,

$$\begin{aligned} \dot{W}_x = \frac{\dot{P}}{\dot{m}} &= -U_2 [W \sin \beta + U] \\ &= -U_2^2 \left[\frac{W \sin \beta + U}{U_2} \right] \\ &= U_2^2 \left[\frac{W \sin(-\beta) - U}{U_2} \right] \end{aligned} \quad A(8)$$

Defining the power conversion efficiency η_c as the fraction of the available power actually converted to shaft work, thus

$$\eta_c = \frac{\dot{P}/\dot{m}}{\dot{P}/\dot{m} + V_2^2/2} \quad A(9)$$

and defining $\beta_2' = -\beta_2$, the relative flow angle at the rim which is positive in the direction of rotation, then

$$\frac{\dot{P}}{\dot{m}} = U^2 \left[\frac{W_2 \sin \beta_2' - U}{U_2} \right]. \quad A(10)$$

From the geometry shown in Figure A1,

$$V_2^2 = V\theta_2^2 + (W_2^2 - [V\theta_2 - U_2]^2)$$

so that,

$$\frac{1}{2}V_2^2 = [U_2 V\theta_2 - \frac{1}{2}U_2^2 + \frac{1}{2}W_2^2] \quad A(11)$$

Using equations A(5) and A(10)

$$-U_2 V\theta_2 = -\dot{W}_x = U^2 \left[\frac{W_2 \sin \beta_2' - U}{U_2} \right] \quad A(12)$$

Substituting equation A(12) into A(11) gives

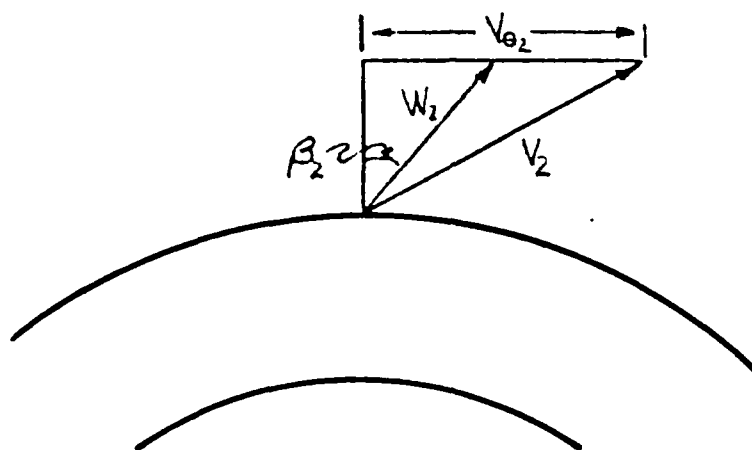


Figure A1. Velocity Triangle of Conventional Cylindrical Flow.

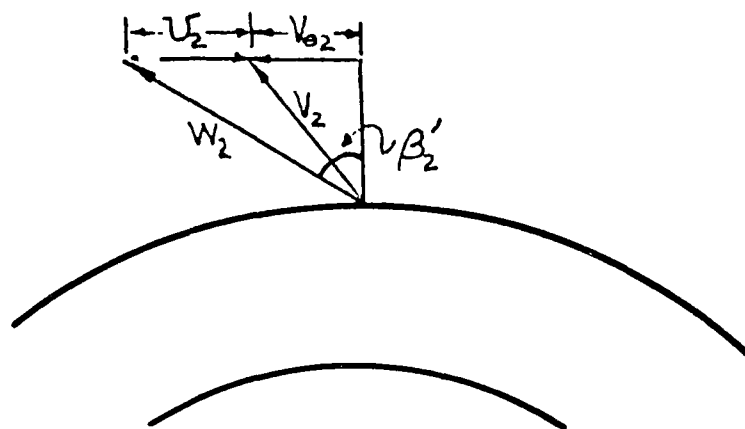


Figure A2. Velocity Diagram at Exit of Rim.

$$P = w' T \quad A(2)$$

The work per unit mass flow is given by

$$P / \dot{m} = w' (r_1 V_{\theta 1} - r_2 V_{\theta 2}) \quad A(3)$$

The subscript 1 denotes entrance station, 2 denotes exit.

Defining the rim speed as $U = rw'$, equation A(3) becomes

$$P / \dot{m} = W_x = U_1 V_{\theta 1} - U_2 V_{\theta 2} \quad A(4)$$

A general velocity diagram for a rotor is shown in Figure A1.

The tangential component of velocity V_{θ} is taken positive in the direction of the rim velocity U . Figure A1 shows all positive velocity components in conventional cylindrical coordinates.

The gas enters the wheel near the center, effectively with zero moment of momentum (about the axial direction).

Therefore $V_{\theta 1} = 0$, and from equation A(4),

$$W_x = \frac{P}{\dot{m}} = -U_2 V_{\theta 2} \quad A(5)$$

For W_x to be positive, it is seen that $V_{\theta 2}$ is negative. The exit velocity diagram representing the flow at the rim of the wheel is given in Figure A2.

From the geometry shown in Figure A1, in general

$$\sin \beta = \frac{V_{\theta} - U}{W} \quad A(6)$$

APPENDIX A

TORQUE PRODUCED BY DISTRIBUTED GAS REACTION

A.1 METHOD

The RDWE concept involves an unsteady process. The potential performance of the RDWE can be understood, approximately, by examining the range of conditions through which the unsteady process passes. Thus the steady flow performance of the proposed arrangement needs to be examined. We first attempt to predict analytically the power or torque impulse that can be generated from the engine under steady flow outlet conditions.

The passages in the RDWE exit nearly tangentially (Figure 1). Since this condition is difficult to achieve we examine the effect of the exit angle on the amount of power that can be generated and the efficiency that can be produced.

The basic equation for relating the fluid flow conditions to the energy transferred to the shaft is Euler's Turbine equation. The torque of the fluid acting on the rotor is given

$$T = \dot{m} (r_1 V_{\theta 1} - r_2 V_{\theta 2}) \quad A(1)$$

If the rotor has a rotational speed w' , the shaft power transferred or rate of work transferred from the fluid to the rotor is given by,

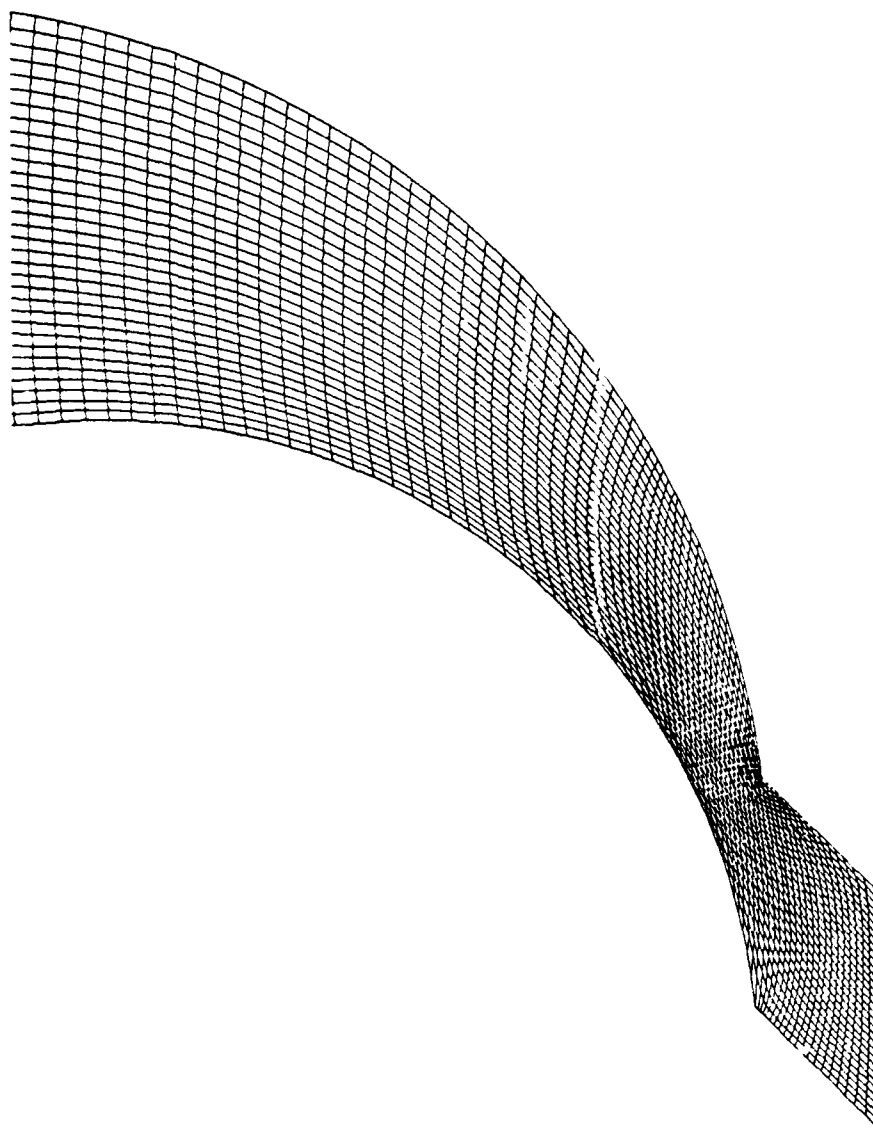


Figure 11. Enlargement of the Grid in the Throat Region.

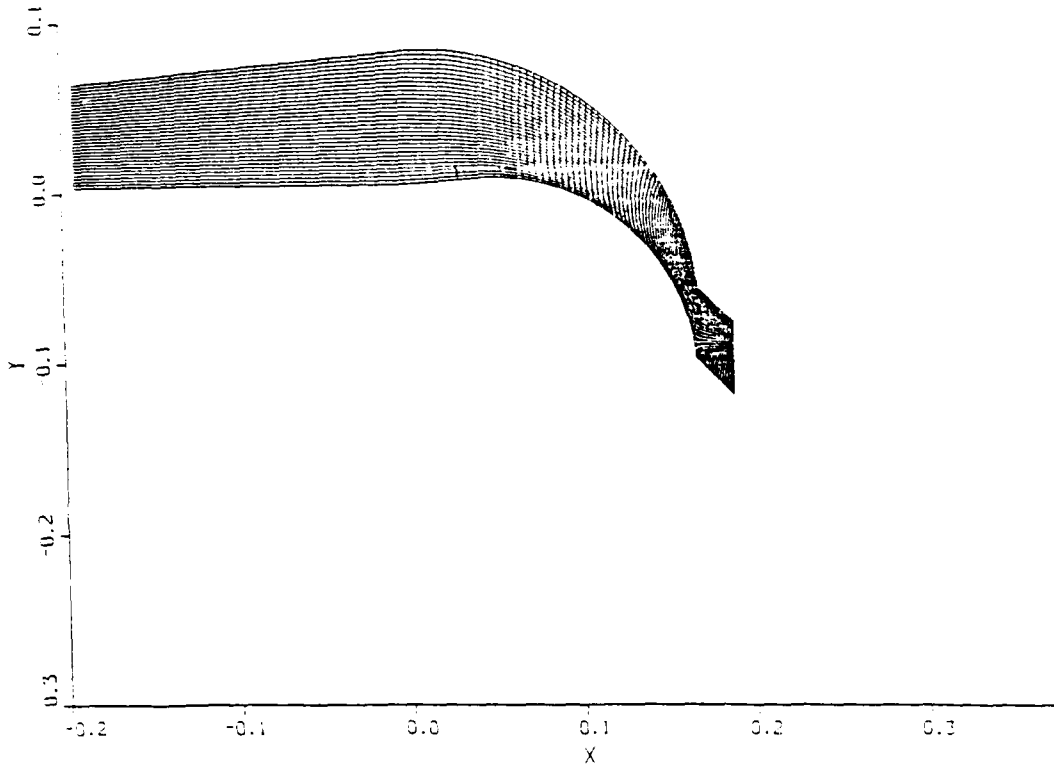
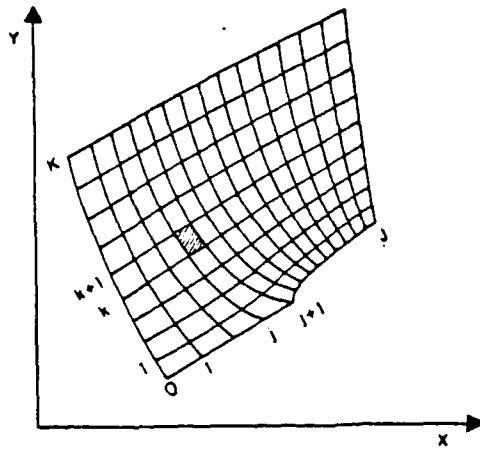
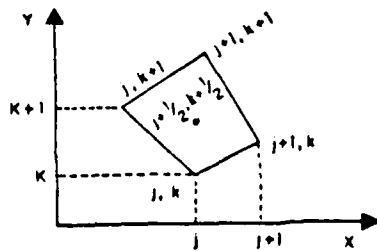


Figure 10. Computational Grid for Outflow Analysis



a) Grid Location in Coordinate System.



b) Single Cell

Figure 9. Computational Grid Notation.

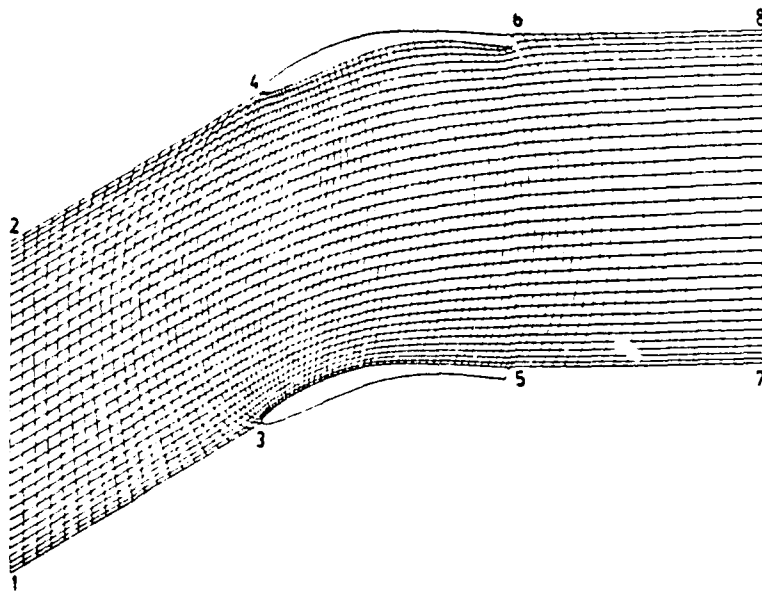
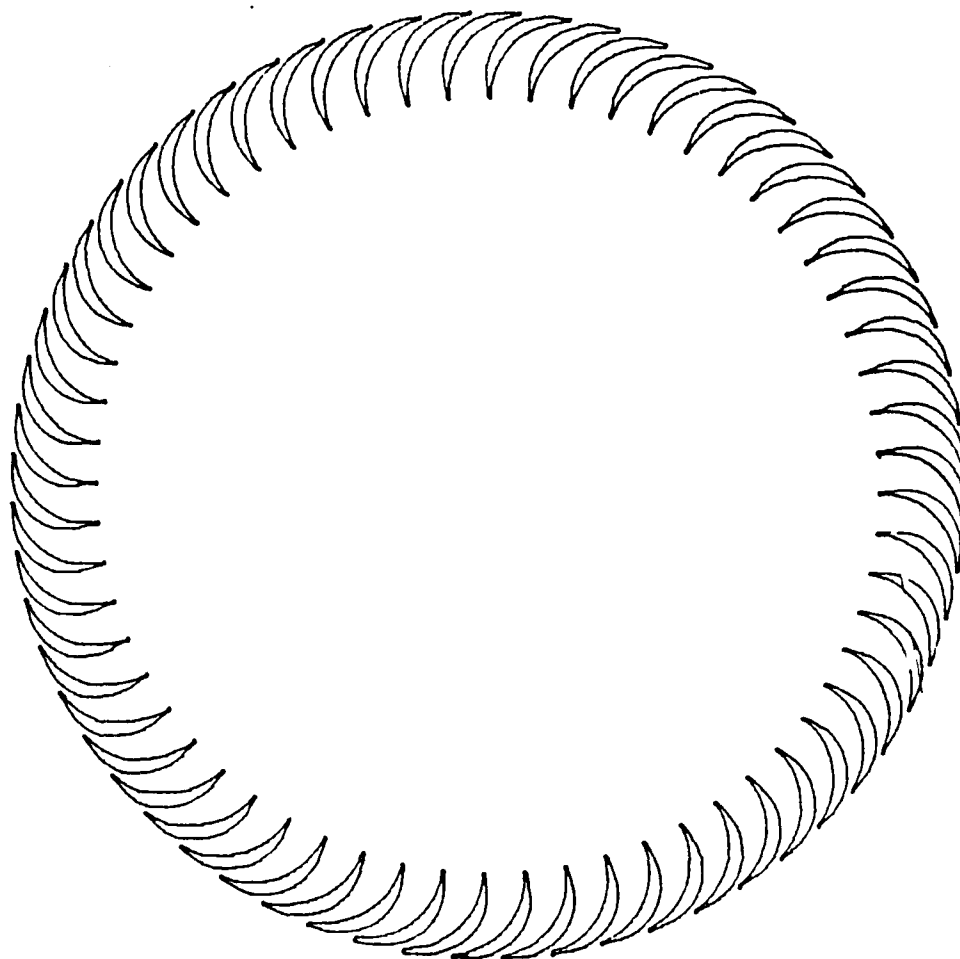


Figure 8. Computational Grid and Boundary of the Computational Domain.



$R_0 = 4$ $R_1 = 3.2$ No. Blades = 60

$k = 9.1.72521902$ $\phi = 80.82738092$

Condition of Tangency is

$\sin \phi = \cos$

$\sin \phi = 0.159407755$ $\cos = 0.159409430$

chord = 0.983540343 chord test = 0.983540073

alpha = 18.34514098

radial solidity = 1.909859317

thickness to chord ratio = 0.194933797

radius of camber circle = 0.758551242

radius of suction circle = 0.575175292

radius of pressure circle = 1.462802226

Figure 7. Final Blading Design.

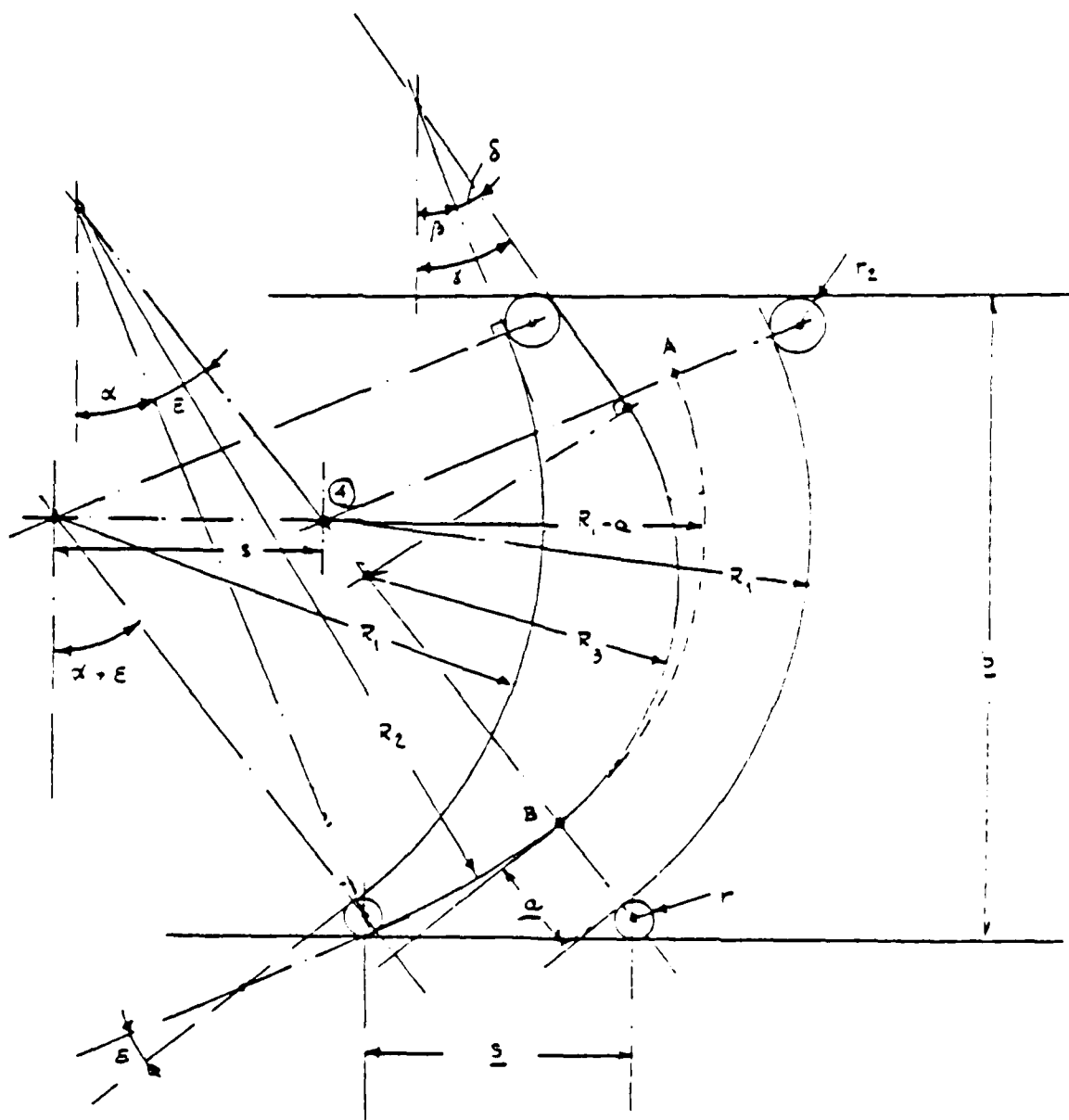


Figure 6. Axial Turbine Blade Geometrical Design.

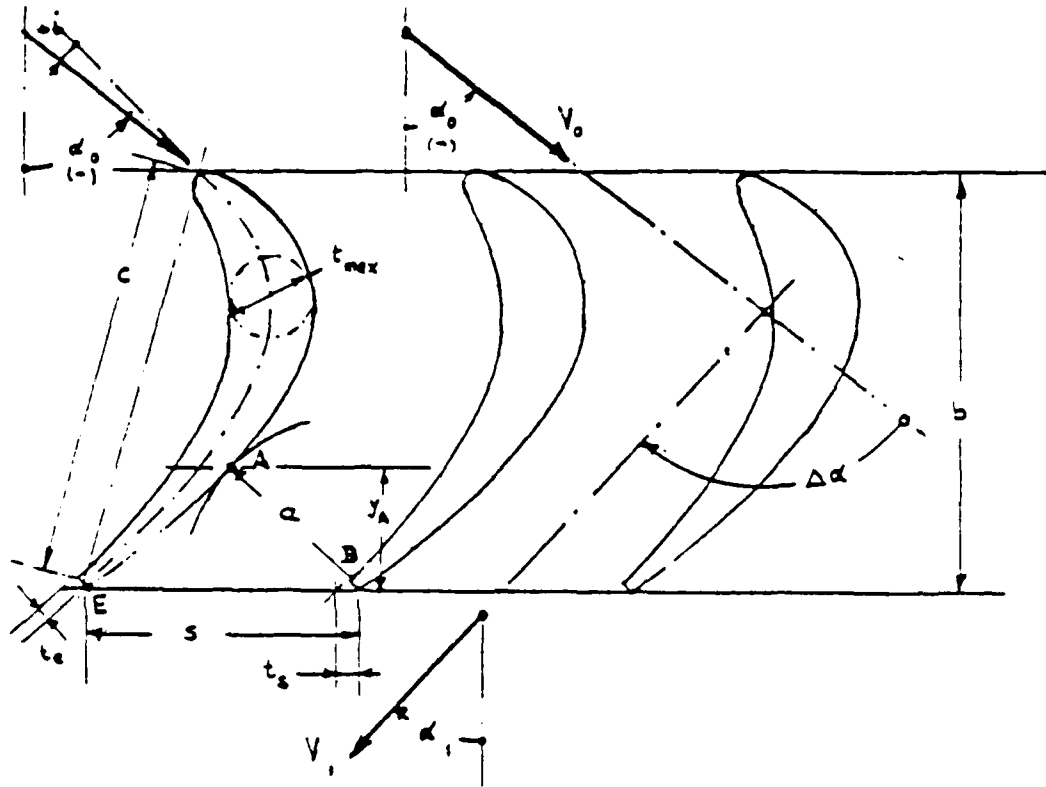
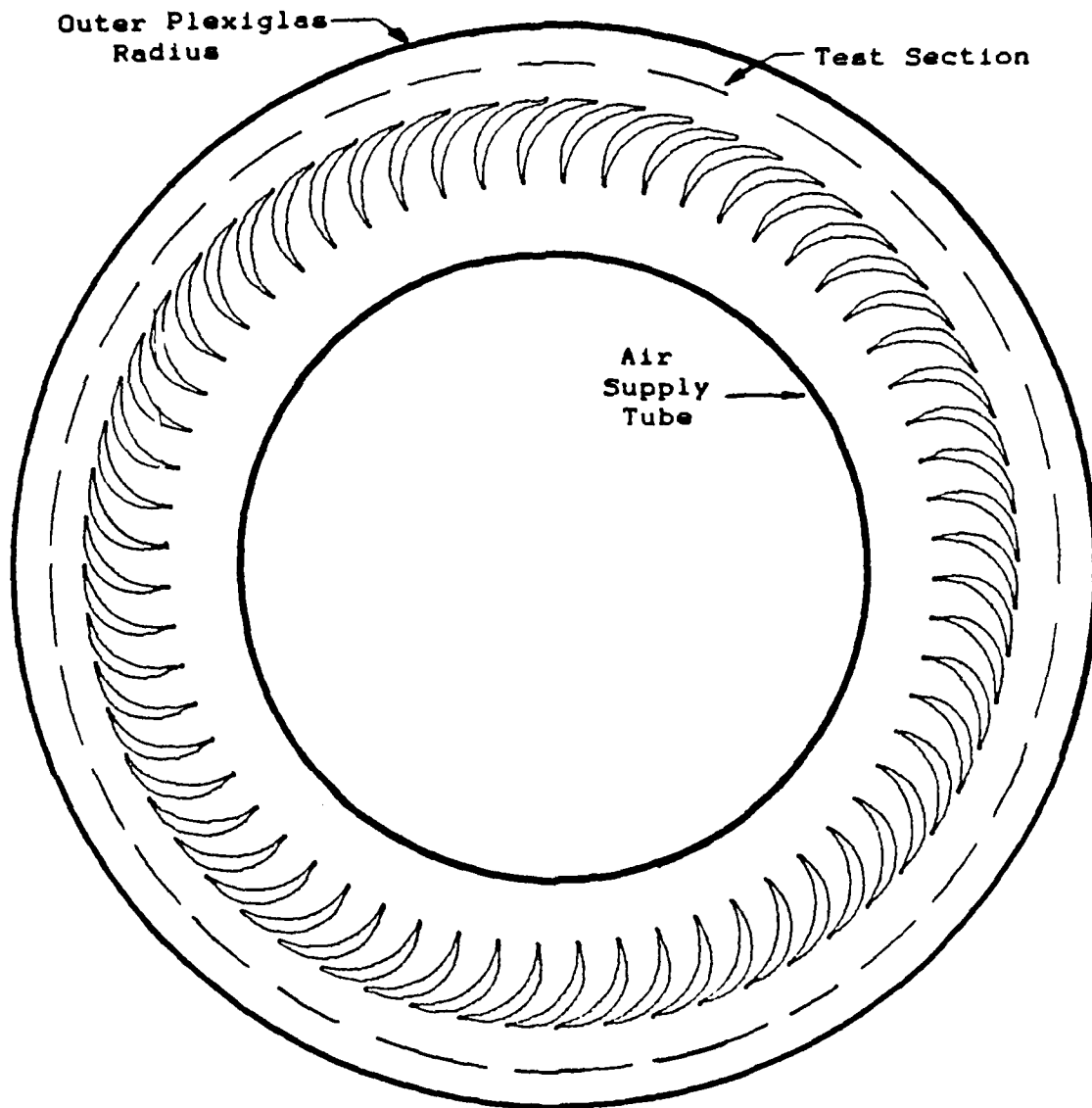


Figure 5. Two-Dimensional Turbine Cascade.



Note: Not to scale.

Figure 4. CDTD Flow Generator - Section AA from Figure 3.

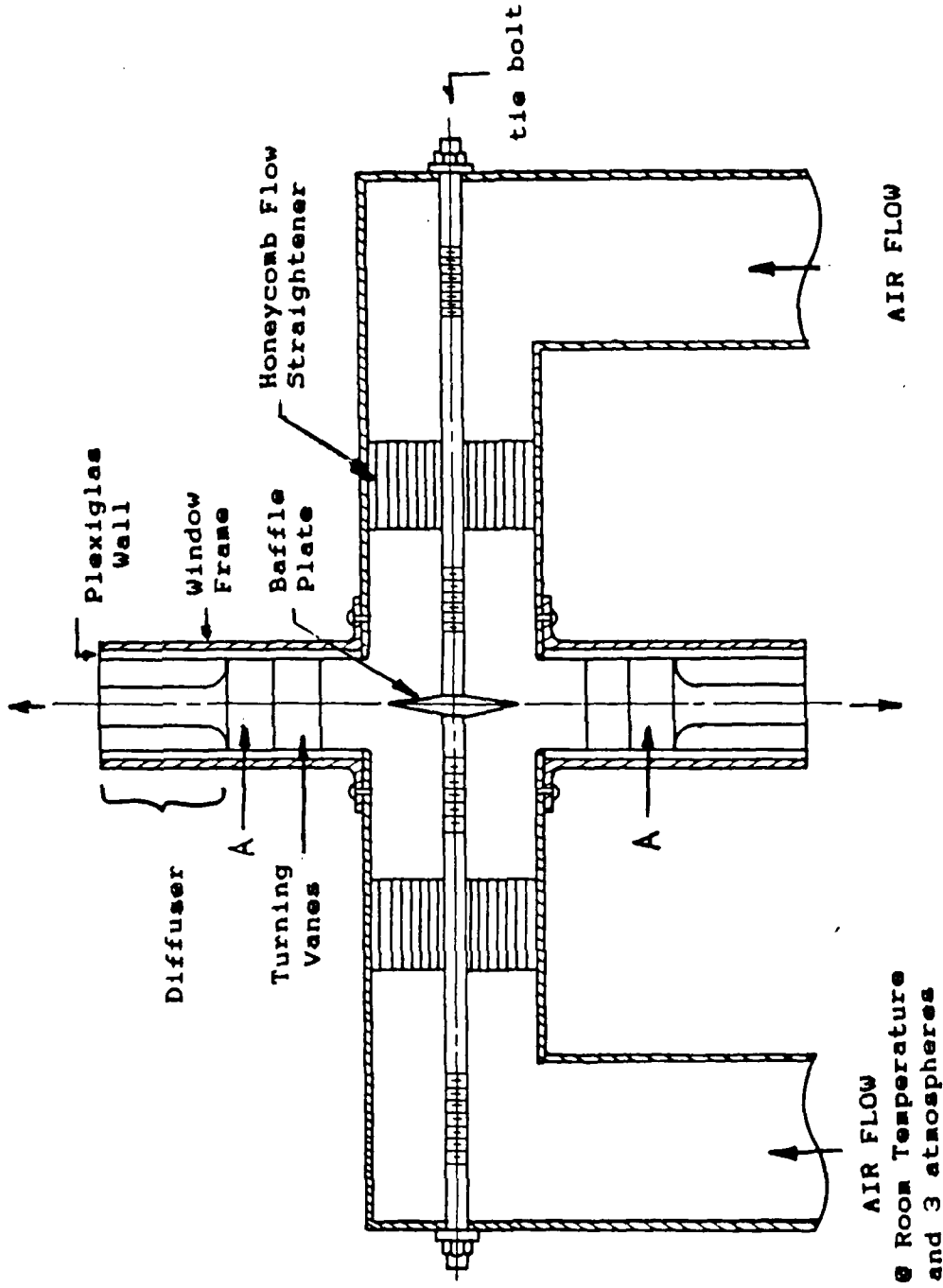


Figure 3. Schematic of the Proposed High Speed CTD.

Thus the conversion efficiency is unity when $w_2/U_2 = 1$ but this is a condition which, from equation A(15) gives zero power output.

A.2 RESULTS

The value of the specific power and conversion efficiency (given by equation A(15) and A(16)) as a function of the ratio of relative flow to wheel velocity, for various values of the relative exit angle, are shown in Figure A3 and Figure A4 respectively.

Figure A3 shows that the specific power increases linearly as the exit velocity increases, and decreases as the relative exit angle becomes less tangential. The conversion efficiency is seen to decrease as the power increases and to decrease as the relative flow angle decreases (less tangential).

The results shown in Figure A3 and Figure A4 can be used to gauge the performance of the unsteady RDWE. In the unsteady expansion process the value of the relative flow angle (β_2) will be constant, being determined by the passage exit geometry. The wheel speed will be approximately constant and only the value of the relative velocity will change. Thus the unsteady process at different times will be described by points on a single line shown on Figure A3 and A4, depending on the particular value of β_2 .

VELOCITY RATIO VS SPECIFIC POWER

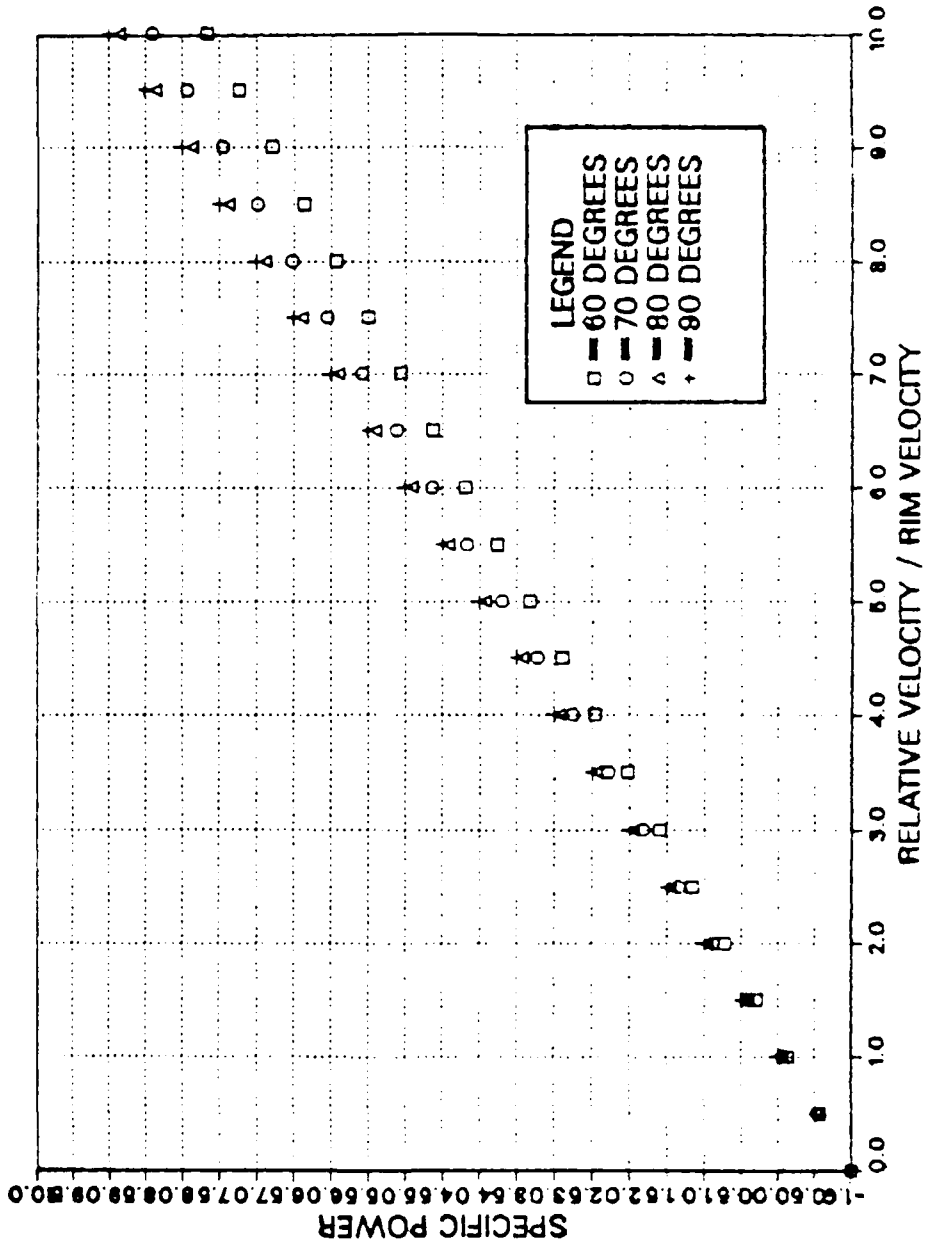


Figure A3. RDWE Specific Power Vs. Velocity Ratio

VELOCITY RATIO VS CONVERSION EFFICIENCY

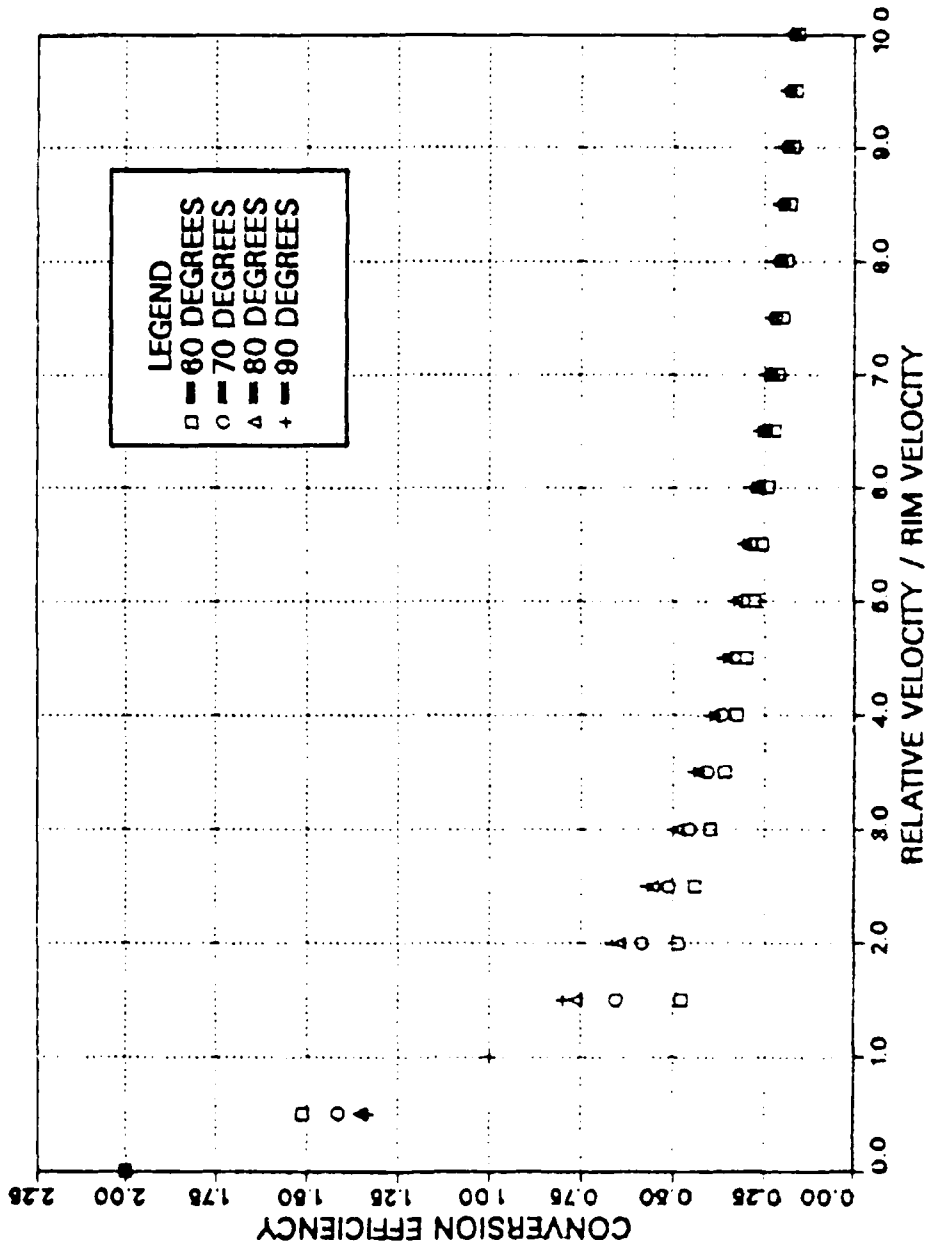


Figure A4. RDWE Power Conversion Efficiency Vs. Velocity Ratio

The difficulty, clearly, is that the exit velocity must not be allowed to decrease below a specific factor times the wheel speed or power will be absorbed rather than generated. Also the conversion efficiency will vary during the expansion, but will always be poor.

This implies that the concept of the RDWE as shown in Figure 1 can not be efficient. The device would require some type of diffuser that would convert the kinetic energy leaving the rotor into static pressure. Unfortunately, a variation in the relative velocity magnitude implies variation in both magnitude and direction of the exit absolute velocity. A suitable diffuser for such a flow does not exist. Consequently, other geometries, particularly those which would allow constant flow to the diffuser by sequencing the detonation wave with (partial) ports at the rotor exit, should be examined.

TABLE A1

Specific Power and Power Conversion Efficiency
Vs Velocity Ratio Data

60 DEG			70 DEG		
W_2/U_2	P_a	η_c	W_2/U_2	P_a	η_c
0	-1	2	0	-1	2
.5	-.56699	1.51200	.5	-.53015	1.4137
1.0	-.13397	∞	1.0	-.06031	∞
1.5	.29904	.47846	1.5	.40953	.65526
2.0	.73205	.48803	2.0	.87938	.58626
2.5	1.16506	.44383	2.5	1.34923	.51399
3.5	2.30109	.36108	3.5	2.28893	.40692
4.5	2.89712	.30099	4.5	3.22862	.33544
5.5	3.76314	.25731	5.5	4.16831	.28501
6.5	4.62917	.22444	6.5	5.10800	.24766
7.5	5.49519	.19892	7.5	6.04770	.21892

80 DEG			90 DEG		
W_2/U_2	P_a	η_c	W_2/U_2	P_a	η_c
0	-1	2	0	-1	2
.5	-.50760	1.35359	.5	-.5	1.33333
1.0	-.01519	∞	1.0	0	1
1.5	.47721	.76354	1.5	.5	.80000
2.0	.96961	.64641	2.0	1.0	.66667
2.5	1.46202	.55695	2.5	1.5	.57143
3.5	2.44683	.43499	3.5	2.5	.44445
4.5	3.43164	.35653	4.5	3.5	.36364
5.5	4.41644	.30198	5.5	4.5	.30769
6.5	5.40125	.26188	6.5	5.5	.26667
7.5	6.38606	.23117	7.5	6.5	.23529

APPENDIX B

DOUBLE CIRCULAR ARC BLADING DESIGN

B.1 METHOD

A computer procedure was developed to design radial out-flow, near tangential turning vanes, specifying only the outer radius, the inner radius, and the number of blades. The blade spacing, radial solidity, camber angle, suction and pressure surface radii, chord length, thickness to chord ratio, and efflux angle are determined. The suction surface is designed to be tangential at the rim.

A Hewlett Packard 9830A computer was used. The blade shapes were generated using a Hewlett Packard 9862A plotter.

The geometrical approach to the design of the vanes is illustrated in Figure B1 and much of the notation is defined in this figure. The following assumptions were made as initial constraints:

1. radius at exit R_0 , is known
2. radius at entrance R_1 , is known
3. number of blades Z , is known
4. The suction side is tangent to the outer radius (point C).
5. The camber line c' , is tangential at the inlet radius (point A).
6. The blade subtends an angle ψ at the center.

Initially, a procedure was developed which required specifying the camber angle θ , R_0 , R_1 , in addition to the number of blades. Since the choice of θ which would give acceptable values of efflux angle and blade thickness was not obvious, an equation for the condition that the camber line was tangent at the rim (which would give a blade of zero thickness, since the suction surface was also required to be tangent) was written. The equation was seen to have two possible roots. The selection of the smaller (incorrect) root gave positive values of the efflux angle and reasonable values of blade thickness. The program which was developed provides the option of selecting θ , or of selecting the blade which results from finding the incorrect smaller root to the tangent camber line condition. Described here are the equations for the generation of the blade shapes.

Defining peripheral blade spacing s as,

$$s = 2 \pi R_0 / Z$$

and the angle subtended by the blade space as

$$\gamma_s = 360 / Z$$

the radial chord as

$$\rho = (R_0 - R_1) / R_0$$

then the radial solidity is given by

$$\sigma_r = (R_0 - R_1) / s = \rho / \gamma_s$$

Using these expressions and Figure B1 the following equations can be written:

$$GE = R_C - R_C \cos (\phi/2) \quad B(1)$$

$$= R_C [1 - \cos (\phi/2)]$$

$$HE = c \tau/2 + R_C [1 - \cos (\phi/2)] \quad B(2)$$

Where τ is the thickness to chord ratio. Also

$$HE = R_s [1 - \cos (\phi_s/2)] \quad B(3)$$

To solve for the thickness and τ we subtract the equations B(1) and B(2)

$$HE - GE = t/2 = \tau c/2 \quad B(4)$$

Using Figure B1,

$$FE = R_C [1 - \cos (\phi/2)] - \tau c/2 \quad B(5)$$

$$= R_p [1 - \cos (\phi_p/2)] \quad B(6)$$

Subtracting equation B(5) from B(1),

$$GE - FE = t/2 = \tau c/2 \quad B(7)$$

The chord c , is given by,

$$c = 2 R_p \sin (\phi_p/2) \quad B(8)$$

$$= 2 R_s \sin (\phi_s/2) \quad B(9)$$

$$= 2 R_C \sin (\phi/2) \quad B(10)$$

All equations were made dimensionless by dividing by R_0 , giving for example

$$c/R_0 = c'' \quad B(11)$$

$$c'' = 2 \frac{R_p}{R_0} \sin (\phi_p/2) \quad B(12)$$

$$= 2 \frac{R_s}{R_0} \sin (\phi_s/2) \quad B(13)$$

$$= 2 \frac{R_c}{R_o} \sin (\phi / 2) \quad B(14)$$

For the geometry we seek, given R_o , and the camber angle ϕ and efflux angle α , the angle ACO (or Ω) is given by

$$\Omega = 90 - (\alpha + \phi/2) \quad B(15)$$

From the triangle ACO

$$\psi + 90 - (\alpha + \phi/2) + 180 - \phi/2 = 180$$

resulting in,

$$90 + \psi = \phi + \alpha \quad B(16)$$

This equation fully defines α . The values of ψ and ϕ are needed to complete the description of the camber line. To solve for the radius of each blade arc the following relations were used.

First with

$$A_s = \frac{R_c}{R_o} - \frac{R_c}{R_o} \cos \phi/2 = HE \quad B(17)$$

and

$$A_p = \frac{R_p}{R_o} - \frac{R_p}{R_o} \cos (\phi_p/2) = FE \quad B(18)$$

Using equation B(3), B(6) and B(7)

$$R_c [1 - \cos (\phi/2)] - R_p [1 - \cos (\phi_p/2)] = r c/2 \quad B(19)$$

Also,

$$A_s - r c/2 - R_p [1 - \cos (\phi_p/2)] = r c/2 \quad B(20)$$

which gives

$$A_p = A_s - r c \quad B(21)$$

Using this relationship between A_s and A_p we can solve for R_s and R_p . From equation B(2), and B(3),

$$A_s = R_s [1 - \cos (\phi_s/2)] \quad B(22)$$

or

$$\cos (\phi_s/2) = 1 - A_s/R_s$$

Squaring and adding together equations B(22), and B(10)

we obtain

$$\cos^2 (\phi_s/2) + \sin^2 (\phi_s/2) = (1 - A_s/R_s)^2 + (c/2R_s)^2$$

or

$$1 = 1 - 2(A_s/R_s) + (A_s/R_s)^2 + c^2/4R_s^2$$

which becomes

$$R_s = \frac{1}{2} A_s + \frac{c^2}{8A_s} \quad B(23)$$

or

$$\frac{R_s}{R_o} = \frac{1}{2} \frac{A_s}{R_o} + \frac{c^2}{8A_s R_o} \quad B(24)$$

Using equations B(5), B(6), and B(16) a similar manipulation will yield,

$$\frac{R_p}{R_o} = \frac{1}{2} \frac{A_p}{R_o} + \frac{c^2}{8A_p R_o} \quad B(25)$$

The angles ϕ_s and ϕ_p are found using equations B(13), and B(14) since

$$\sin (\phi_s/2) = c/2R_s$$

or

$$\phi_s = 2 \arcsin \left(\frac{c/R_o}{2R_s/R_o} \right) \quad B(26)$$

and similarly

$$\sin (\phi_p/2) = c/2R_p$$

or

$$\phi_p = 2 \arcsin \left(\frac{c/R_o}{2R_p/R_o} \right) \quad B(27)$$

The desired condition is that the suction surface be tangent to the outer rim. From Figure B1 this is given by the relation

$$\phi_s/2 = \alpha + \phi/2 \quad B(28)$$

r is not an independent parameter since it can be calculated using equation B(25), thus

$$r = \frac{[(R_s [1 - \cos (\phi_s/2)] - R_o [1 - \cos (\phi/2)])]}{(c/2)} \quad B(29)$$

To insure near tangential flow at the exit we first seek the condition of a tangent camber line at the exit. This implies since we also seek a tangent suction surface, that the blade would have zero thickness. Using the notation in Figure B2 the following equations apply:

$$\sin (\phi/2) = L / c \quad B(30)$$

and

$$\sin \psi = L / R_o \quad B(31)$$

Substituting equation B(30) into B(31) gives,

$$c = \frac{R_o \sin \psi}{\sin (\phi/2)} \quad B(32)$$

From the geometry

$$\cos (\phi / 2) = y / c \quad \text{B(33)}$$

and

$$\cos \psi = \frac{R_i + y}{R_o} \quad \text{B(34)}$$

or

$$R_o \cos \psi = R_i + y \quad \text{B(35)}$$

Substituting equation B(33) into B(35) gives,

$$R_o \cos \psi = R_i + c \cos (\phi / 2) \quad \text{B(36)}$$

or

$$R_o \cos \psi - R_i = c \cos (\phi / 2) \quad \text{B(37)}$$

Equation B(32) can be rewritten such that,

$$R_o \sin \psi = c \sin (\phi / 2) \quad \text{B(38)}$$

and dividing equation B(38) by B(39),

$$\frac{R_o \sin \psi}{R_o \cos \psi - R_i} = \tan (\phi / 2) \quad \text{B(39)}$$

This equation establishes the relationship between ψ and ϕ . Using Figure B3 the relationship of c , ψ , ϕ is established,

$$\cos (\phi / 2) = \frac{c / 2}{R \tan \psi} \quad \text{B(40)}$$

or

$$c = 2 R_o \tan \psi \cos (\phi / 2) \quad \text{B(41)}$$

This is the condition for the camber line to be tangent at the exit.

Using equations B(32) and B(41),

$$\frac{\sin \psi}{\sin(\phi/2)} = 2 \tan \psi \cos(\phi/2) \quad \text{B(42)}$$

giving,

$$\begin{aligned} \cos \psi &= 2 \sin(\phi/2) \cos(\phi/2) \\ &= 2 \left[\frac{1}{2} \sin(\phi/2 + \phi/2) + \sin(\phi/2 - \phi/2) \right] \\ &= \sin \phi \end{aligned} \quad \text{B(43)}$$

Therefore for the camber line tangency condition

$$\cos \psi = \sin \phi \quad \text{B(44)}$$

Using equation B(39) and B(44) we obtain the following

$$\frac{2 \sin(\phi/2) \cos(\phi/2)}{2 \cos^2(\phi/2)} = \tan(\phi/2)$$

and

$$\frac{2 \sin(\phi/2) \cos(\phi/2)}{2 \cos^2(\phi/2)} = \frac{R_o \sin \psi}{R_o \cos \psi - R_i}$$

Using the general trigonometrical relationship,

$$\sin 2x = 2 \sin x \cos x$$

we can manipulate the preceding equation to obtain

$$\frac{\sin \phi [R_o \cos \psi - R_i]}{R_o \sin \psi} = 2 \cos^2(\phi/2) \quad \text{B(45)}$$

Using equation B(43) this becomes

$$\cos \psi [R_o \cos \psi - R_i] = 2 \cos^2(\phi/2) \quad \text{B(46)}$$

Using the relationship

$$\begin{aligned} \cos^2 x &= \sin^2 x + \cos 2x \\ 2 \cos^2(\phi/2) &= 2 [\sin^2(\phi/2) + \cos \phi] \\ &= 2 \left[\frac{1 + \cos \phi}{2} \right] \end{aligned}$$

$$= 1 + (1 - \sin^2 \phi)^{1/2}$$

Using equation B(43) this becomes,

$$\begin{aligned} 2 \cos^2 (\phi/2) &= 1 + (1 - \cos 2\phi)^{1/2} \\ &= 1 + \sin \psi \end{aligned} \quad \text{B(47)}$$

This gives

$$R_0 \cos^2 \psi - R_i \cos \psi = R_0 \sin \psi + R_0 \sin^2 \psi \quad \text{B(48)}$$

Writing $s = \sin \psi$ equation (48) becomes,

$$R_0(1 - s^2) - R_i (1 - s^2)^{1/2} = R_0 s + R_0 s^2 \quad \text{B(49)}$$

or

$$\begin{aligned} \frac{R_0}{R_i} [(1 - s^2) - s^2 - s] &= -(1 - s^2)^{1/2} \\ \left(\frac{R_0}{R_i} \right)^2 [1 - 2s - 3s^2 + 4s^3 + 4s^4] &= 1 - s^2 \end{aligned}$$

Thus equation B(48) gives the condition

$$F(s) = \frac{(R_i)^2}{R_0} (1 - s^2) - 1 + s(2 + 3s - 4s^2 - 4s^3) = 0 \quad \text{B(50)}$$

The condition of tangency of the camber line is given by the solution of equation B(50) for s between 0 and 1, since $s = \sin \psi$. Using Newton's method of iteration the root can be found for a given radius ratio. Figure B4 shows $F(s)$ in equation B(50) for various radius ratios. Figure B4 clearly identifies two possible roots. The larger root is the correct root, giving zero blade thickness. The smaller root is incorrect, but gives positive values of α and finite blade thickness. Emphasis was placed on finding the first

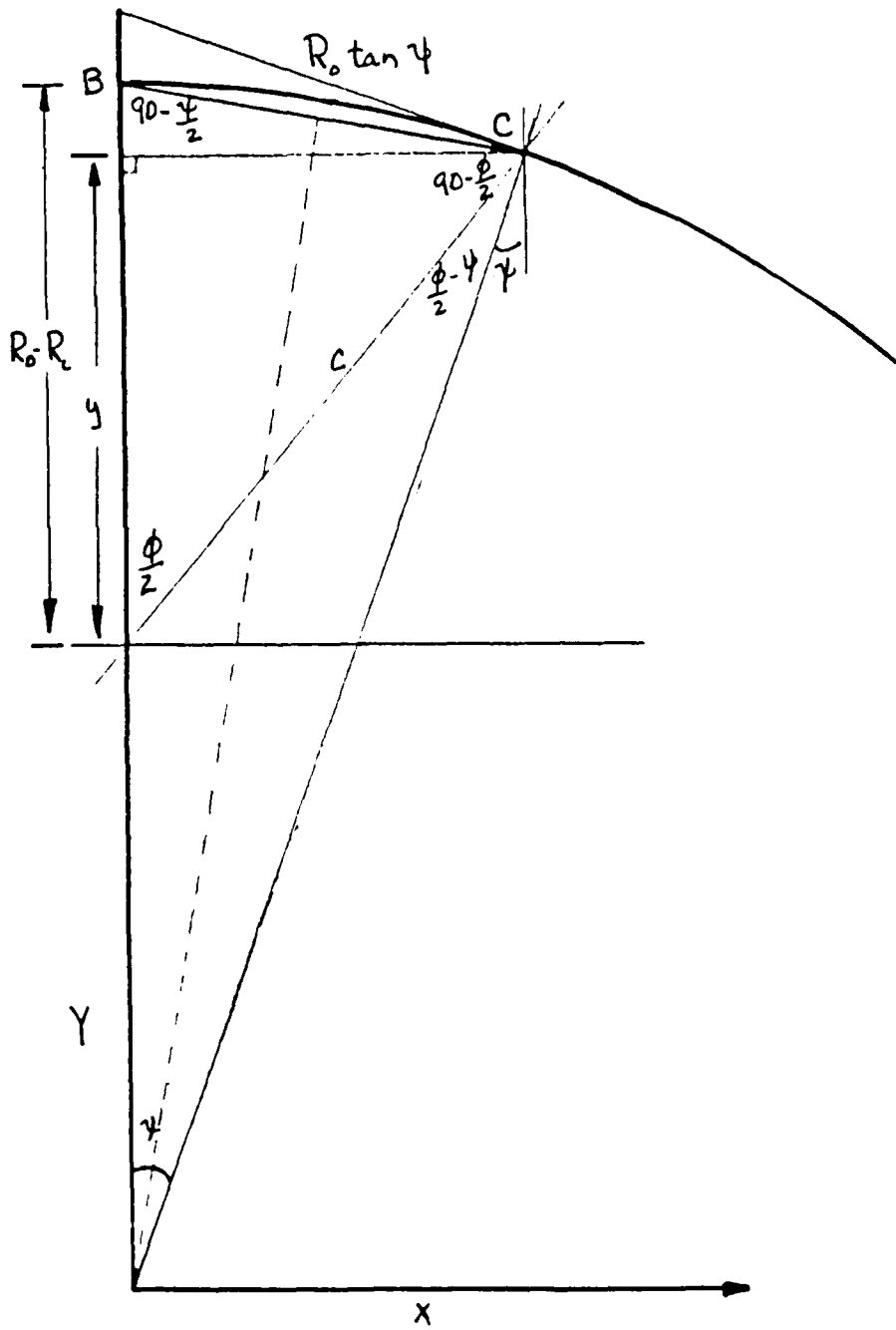


Figure B2. Geometrical Description for Camber Line Tangency Condition.

TABLE B1. List of Computer and Text Symbols for
Double Circular Arc Blades (con't)

"ACIRC"	TEXT	IDENTIFICATION
T1	τ	thickness to chord ratio
T2	θ_s	suction angle
T3	θ_p	pressure angle
T4	θ	loop parameter to draw arcs
T9	-	tolerance on Newtons method of integration
X1	x_{ds}	suction center x coordinate
X2	x_{dP}	pressure center x coordinate
X3	x_d	camber center x coordinate
X4	-	variable for x values in continuous loop
X9	-	variable for x values in rotational loop
Y1	y_{ds}	suction center y coordinate
Y2	y_{dP}	pressure center y coordinate
Y3	y_d	camber center y coordinate
Y4	-	variable for y values in continuous loop
Y9	-	variables for y values in rotational loop
Z0	Z	number of blades

TABLE B1. List of Computer and Text Symbols for
Double Circular Arc Blades (con't)

"ACIRC"	TEXT	IDENTIFICATION
02	$\cos \psi$	$\cos \psi$
03	R_C	output print of R_C
04	R_S	output print of R_S
05	sin	for tangent test
06	$\cos \theta$	for tangent test
P1	π	π
P4	-	constant, $cR_0/2R_p$
R0	R_0	outer radius
R1	R_1	inner radius
R2		density, $(R_0 - R_1)/R_0$
R3	R_C/R_0	camber radius, dimensionless
R4	R_1/R_0	inner radius, dimensionless
R5	R_S/R_0	suction radius, dimensionless
R6	R_p/R_0	pressure radius, dimensionless
S0	ψ_s	periodicity, $2\pi R_0/Z$
S1	σ_r	radial solidity
S2	s	spacing
S3	ψ	blade curvature with respect to camber line
S5	ψ_s	periodicity, $360/Z$
T0	θ	camber angle

TABLE B1. List of Computer and Text Symbols
for Double Circular Arc Blades

"ACIRC"	TEXT	IDENTIFICATION
A0	α	efflux angle
A1	A_s	suction line to chord length
A2	A_p	pressure line to chord length
C0	c''	c/R_0 dimensionless parameter for chord length
C1	c	chord length
C2	c	chord length for tangent test
I1	-	Interval ($\phi/2 - \phi_s/2$)
I2	-	Interval ($\phi/2 + \phi_s/2$)
I3	-	Interval ($\phi/2 + \phi_s/2$) - ($\phi/2$ - $\phi_s/2$)
K1	-	constant value
K2	-	Newtons method, y/y'
K9	-	initial guess for Newton's method
L	-	counter
N	N	Number of blades to draw
NO	-	Number of blades to draw for loop
N9	-	Number of points for interval of arc
O1	-	Equals 1 for solution of $\psi, 2$ for input ψ

```
1390 K9=0.1
1400 DEF FNF(K9)=(1-R4↑2)+(1-K9↑2)-K9*(2+2+K9-4+K9↑2-4+K9↑3)
1410 DEF FND(K9)=- (6*K9-2*K9+R4↑2+12*K9↑2+16*K9↑3)-2
1420 K1=K9
1430 K2=FNF(K9)/FND(K9)
1440 K9=K1-K2
1450 IF ABS(K2)>ABS(K9*T9) THEN 1420
1460 RETURN
```

```

910 Y3=R4
920 REM****DRAW BLADE SURFACES****
930 DISP "INPUT THE NUMBER OF BLADES TO DRAW";
940 WAIT 1000
950 DISP " ";
960 DISP "STARTING AT N=1";
970 INPUT N
980 REM-----EDIT NEXT LINE FOR PLOT RESOLUTION-----
990 N9=25
1000 FOR N0=1 TO N
1010 I1=(T0/2)-(T2/2)
1020 I2=(T0/2)+(T2/2)
1030 I3=(I2-I1)/N9
1040 REM***FOR THE SUCTION SIDE***
1050 FOR T4=I1 TO I2 STEP I3
1060 X4=X1-(R5*COS(T4))
1070 Y4=Y1+(R5*SIN(T4))
1080 X9=X4*COS((N0-1)*95)+(Y4*SIN((N0-1)*95))
1090 Y9=Y4*COS((N0-1)*95)-(X4*SIN((N0-1)*95))
1100 PLOT X9,Y9
1110 NEXT T4
1120 PEN
1130 REM***FOR CAMBER LINE***
1140 FOR T4=0 TO T0 STEP T0/N9
1150 X4=X3-(R3*COS(T4))
1160 Y4=Y3+(R3*SIN(T4))
1170 X9=X4*COS((N0-1)*95)+(Y4*SIN((N0-1)*95))
1180 Y9=Y4*COS((N0-1)*95)-(X4*SIN((N0-1)*95))
1190 PLOT X9,Y9
1200 NEXT T4
1210 PEN
1220 REM***FOR PRESSURE SIDE***
1230 I4=T0/2-T3/2
1240 I5=T0/2+T3/2
1250 I6=(I5-I4)/N9
1260 FOR T4=I4 TO I5 STEP I6
1270 X4=X2-(R6*COS(T4))
1280 Y4=Y2+(R6*SIN(T4))
1290 X9=X4*COS((N0-1)*95)+Y4*SIN((N0-1)*95)
1300 Y9=Y4*COS((N0-1)*95)-X4*SIN((N0-1)*95)
1305 PLOT X9,Y9
1310 NEXT T4
1320 PEN
1330 NEXT N0
1335 REM*****
1340 END
1350 REM****NEWTONS WILL BE USED TO CALCULATE***
1360 REM****TANGENCY FOOT BETWEEN 0 & 90 DEGREES*****
1370 REM****SOLVING FOR THE 1ST FOOT*****
1380 T9=0.00001

```

```

430 C2=2*TANS3+COS(T0/2)*R0
430 REM*****CONCLUDES CALCULATION FOR PSI,PHI,AND C*****
440 A0=90+S3-T0
450 C0=C1/R0
460 R3=C0/(2*SIN(T0/2))
470 R4=R1/R0
480 D0=ATN(R3/R4)
485 REM*****
490 REM****FOR SUCTION SURFACE TANGENT TO OUTER RIM****
500 T2=(2*A0)+I0
510 R5=C0/(2*SIN(T2/2))
520 T1=((R5*(1-COS(T2/2)))-(R3*(1-COS(T0/2))))/(C0/2)
530 A1=R3*(1-COS(T0/2))+C0*T1/2
540 A2=A1-(C0*T1)
550 IF A2>0 THEN 640
560 IF L=1 THEN 620
570 DISP "NO SOLUTION-RI IS TOO SMALL";
580 DISP " ";
590 DISP "H INCREASES RI I.E.=25% ENTER H";
600 INPUT H
610 L=1
620 R1=R1+(H/100)
630 GOTO 200
640 R6=(A2/2)+(C0+2/(8*A2))
650 P4=C0/(2+R6)
660 T3=2*ATN(P4/SQR(1-P4+2))
670 O3=R3+R0
680 O4=R5+R0
690 O1=R6+R0
695 REM*****
700 REM*****PRINT STATEMENTS*****
710 PRINT "R0="R0"RI="R1"NO. BLADES="Z0
720 PRINT "PSI="S3
730 PRINT "PHI="T0
740 PRINT "CONDITION FOR TANGENCY IS"
750 PRINT " SIN PHI=COS PSI"
760 PRINT " SIN PHI ="O5" COS PSI ="O6
770 PRINT "CHORD="C1"CHORD TEST="C2
780 PRINT "ALPHA="A0
790 PRINT "RADIAL SOLIDITY="R9
800 PRINT "THICKNESS TO CHORD RATIO="T1
810 PRINT "RADIUS OF CAMBER CIRCLE ="O3
820 PRINT "RADIUS OF SUCTION CIRCLE ="O4
830 PRINT "RADIUS OF PRESSURE CIRCLE="O1
840 REM*****END PRINT STATEMENTS*****
845 REM*****
850 REM****CENTERS CAN NOW BE DETERMINED****
860 X1=R3-((R3*COS(T0/2))-(R5*COS(T2/2)))*COS(T0/2)
870 Y1=R4+((R3*COS(T0/2))-(R5*COS(T2/2)))*SIN(T0/2)
880 X2=R3+((R6*COS(T3/2))-(R3*COS(T0/2)))*COS(T0/2)
890 Y2=R4-((R6*COS(T3/2))-(R3*COS(T0/2)))*SIN(T0/2)
900 X3=R3

```

B.2.4 Program Listing

Listed here is the program listing, "ACIRC" for the design of double circular arc blades

```
10 REM*****ACIRC 1 JUNE 1984*****
20 REM*****PROGRAM TO CALCULATE & DRAW ARC BLADING*****
30 REM*****FOR AN INITIALLY OUTFLOW CASCADE*****
40 REM*****USING NEWTONS METHOD TO SOLVE FOR THE*****
50 REM*****OF PSI*****
60 DEG
70 SCALE -1,1,-1,1
80 DISP "SET PLOTTER 7(X) BY 7(Y)-<CONT>";
90 STOP
95 REM*****INPUT DATA*****
100 DISP "ENTER THE OUTER RADIUS";
110 INPUT R0
120 DISP "ENTER THE INNER RADIUS";
130 INPUT R1
140 R4=R1/R0
150 DISP "ENTER THE NUMBER OF BLADES";
160 INPUT Z0
170 L=0
180 REM*****END INPUT DATA****
185 REM*****CALCULATIONS*****
190 S5=360/Z0
200 P1=3.141592654
210 S2=2*P1*R0/Z0
215 R9=(R0-R1)/S2
220 S1=(R0-R1)/S2
230 S0=S2/R0
240 R2=S0*S1
250 DISP "WANT PSI CALCULATED Y=1,0=N";
260 WAIT 1000
270 INPUT O1
280 IF O1=1 THEN 340
290 DISP "INPUT PSI";
300 INPUT S3
310 O2=COSS3
320 T0=ATH(O2/SQR(1-O2^2))
330 GOTO 380
340 GOSUB 1350
350 REM*****NOW DETERMINE THE VALUES FOR PSI,PHI,AND C*****
360 S3=ATH(K9/SQR(1-K9^2))
370 T0=2*ATH(R0*SINS3/(R0*COSS3-R1))
380 O5=SINS3
390 O6=COST0
400 C1=R0*SINS3/SIN(T0/2)
405 REM*****
410 REM*****TEST FOR TANGENCY*****
```

Chord length

Angle α

Thickness to chord ratio

Radius of camber line

Radius of suction line

Radius of pressure line

is a convex arc. To remedy this, the program asks the user to increase the dimension on the inner radius by a percentage. The program will use this value to solve for the required inner radius to achieve a suction surface that is tangent to the outer rim.

The fifth part prints the output. The sixth part draws the blade surfaces.

B.2.2 Required Inputs

The following inputs are requested:

Outer radius

Inner radius

Total number of Blades

Yes or No response for solving for the value of γ

Percentage increase in the inner radius - may

be required, when the value of γ is specified

Number of Blades requested to be drawn

B.2.3 Listed Outputs

The following outputs are listed:

Outer radius

Inner radius

Number of Blades

Angle γ

Angle θ

Results of test for tangency

illustrates the computer generated shapes and passage for a 60 blade design.

B.2 COMPUTER PROGRAM "ACIRC"

B.2.1 Description

A computer program, "ACIRC" was written to construct double circular arc blading using the above procedure. The program will calculate and draw blading for a initially radial-outflow using Newtons Method to solve for a suitable value of ψ , or for an arbitrary input value of ψ . In either case the method will yield a suction surface which is tangent to the outer rim.

The program is user friendly and is annotated for ease of understanding. The program is divided into six major parts.

The first part is the input data section. The second part calculates the periodicity, radial solidity, spacing, and asks the user if the value of ψ is to be calculated or to be specified.

The third part calculates the first root for tangency conditions at the exit. No input is required for this section. The fourth part calculates the parameters needed for the suction surface to be tangent to the outer rim. Usually, if the user specified a value of ψ there is the possibility of the distance from the chord to the pressure circle being negative. If this occurs the result

$$\begin{aligned}
 x_d &= R_c \\
 &= R_c/R_o \\
 y_d &= R_1 \\
 &= R_1/R_o
 \end{aligned}$$

To draw successive blades on a rotor the program must rotate the axes about the rotor center after each blade is drawn. The following equations were used (see Figure B5).

$$\begin{aligned}
 X &= \frac{x}{\cos \theta} + Y \frac{\sin \theta}{\cos \theta} \\
 \frac{Y}{\cos \theta} + x \frac{\sin \theta}{\cos \theta} &= y
 \end{aligned}$$

therefore,

$$\begin{aligned}
 X &= x \cos \theta + y \sin \theta \\
 Y &= y \cos \theta - x \sin \theta
 \end{aligned}$$

Given the number of blades, the following operations (for all three arcs) are performed, the coordinates are calculated as

$$\begin{aligned}
 x &= x_d, ds, dp - R \cos \theta \\
 y &= y_d, ds, ds + R \sin \theta
 \end{aligned}$$

The arcs are then drawn from $\theta = ((\phi/2) - (\phi_s, p/2))$ to $((\phi/2) + (\phi_s, p/2))$

using

$$X = x \cos (N) \frac{360}{Z} + y \sin (N) \frac{360}{Z}$$

and

$$Y = y \cos (N) \frac{360}{Z} - x \sin (N) \frac{360}{Z}$$

where N is the number of blades. Figure B6 and B7

root. The value found will give the selected value of $\sin \gamma$. Once γ is found, using equation B(39) ϕ can be calculated and c is obtained using equation B(32).

Using equation B(28) and B(9) ϕ_s and R_s can be calculated and the thickness is then given using equation B(29).

A test is made to assure that the length A_p is positive. If A_p is negative this implies a convex rather than concave pressure side. This would also imply that the inner radius is too small and should be increased to produce concave curvature on the pressure side. A_p is found, from equations B(19) and B(16).

The alternate procedure did not require the camber line to be tangent at the exit. In this case the value of γ is not solved for but is left as an input parameter. The values of ϕ and c are then found directly using equation B(39).

The centers of curvature are given by,

$$x_{ds} = \frac{R_c}{R_o} - \left(\frac{R_c}{R_o} \cos(\phi/2) - \frac{R_s}{R_o} \cos(\phi_s/2) \right) \cos(\phi/2)$$

$$y_{ds} = \frac{R_i}{R_o} + \left(\frac{R_c}{R_o} \cos(\phi/2) - \frac{R_s}{R_o} \cos(\phi_s/2) \right) \sin(\phi/2)$$

$$x_{dp} = \frac{R_c}{R_o} + \left(\frac{R_p}{R_o} \cos(\phi_p/2) - \frac{R_c}{R_o} \cos(\phi/2) \right) \cos(\phi/2)$$

$$y_{dp} = \frac{R_i}{R_o} - \left(\frac{R_p}{R_o} \cos(\phi_p/2) - \frac{R_c}{R_o} \cos(\phi/2) \right) \sin(\phi/2)$$

with

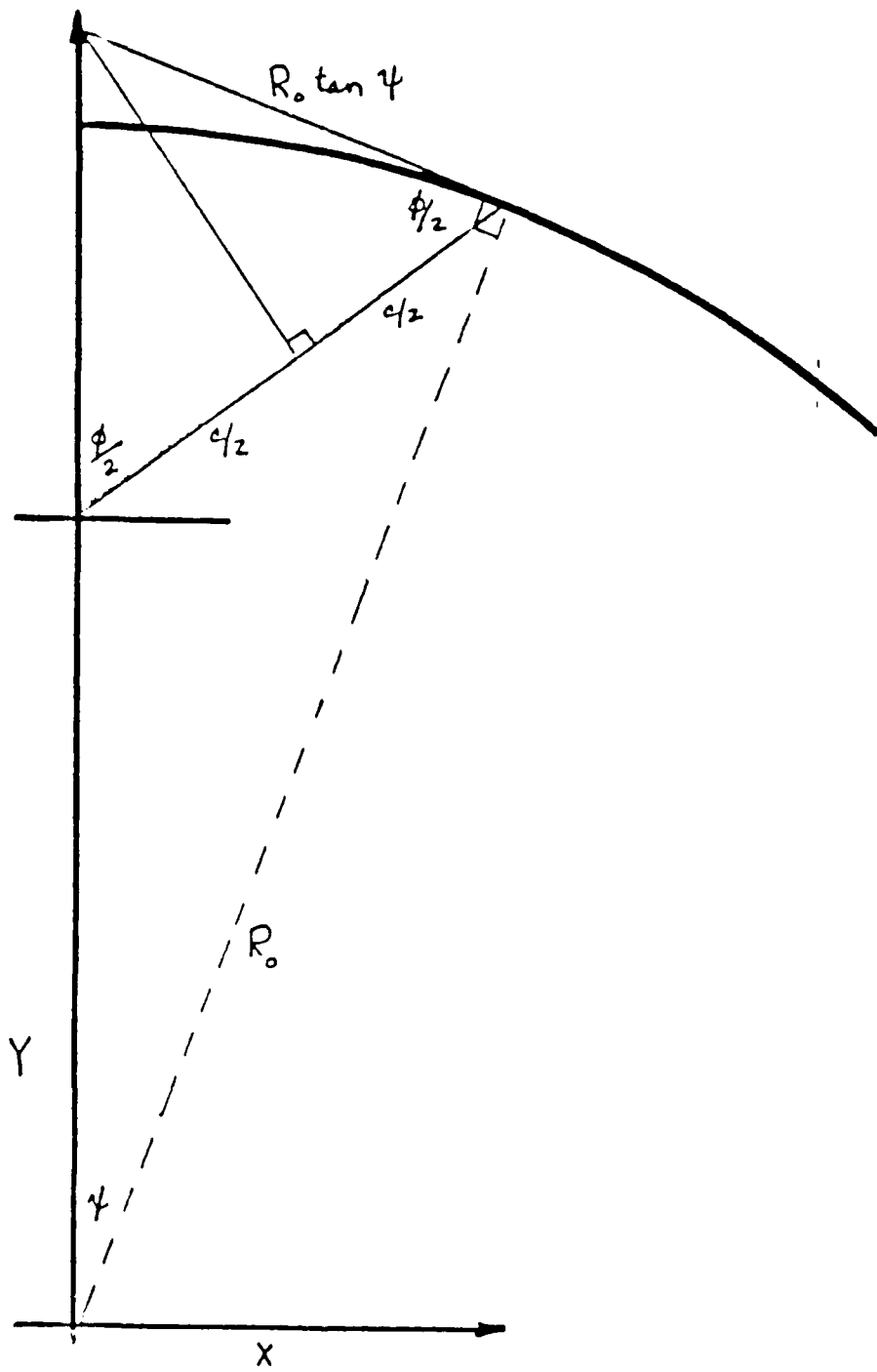


Figure B3. Continued Geometrical Description for Camber Line Tangency Condition

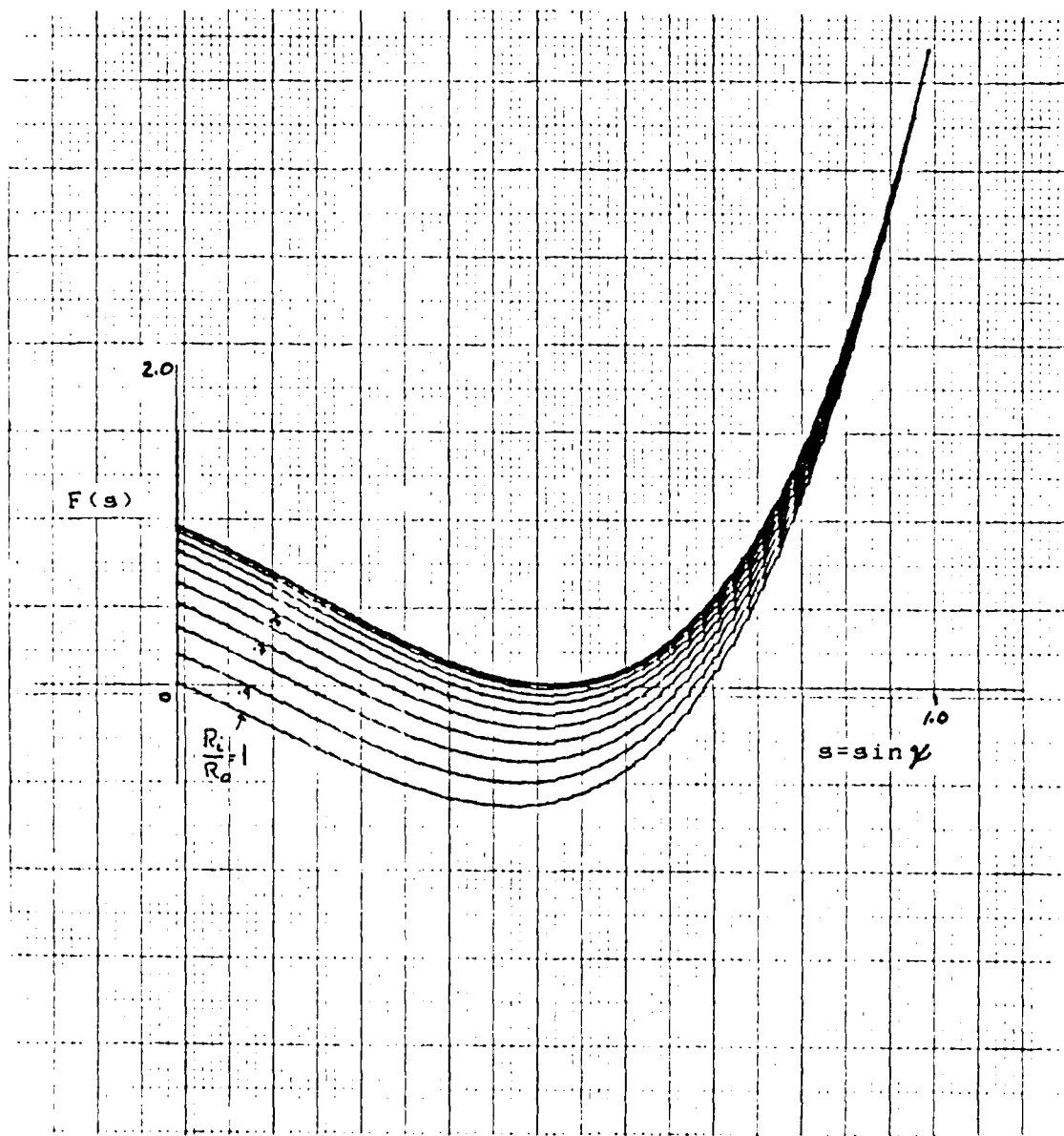


Figure B4. Function of ψ Resulting from the Condition of Tangency of the Camber Line (equation B(50)).

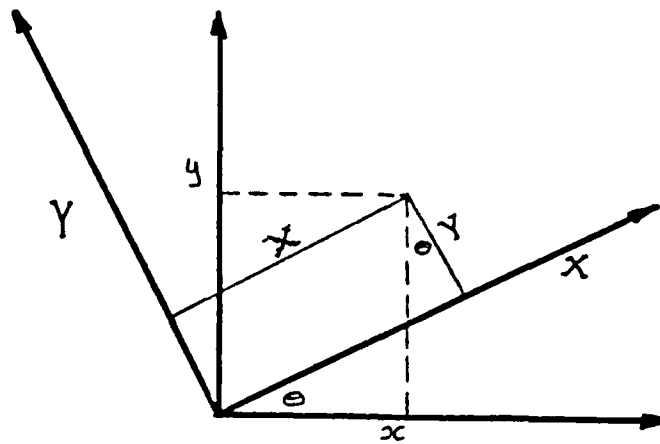
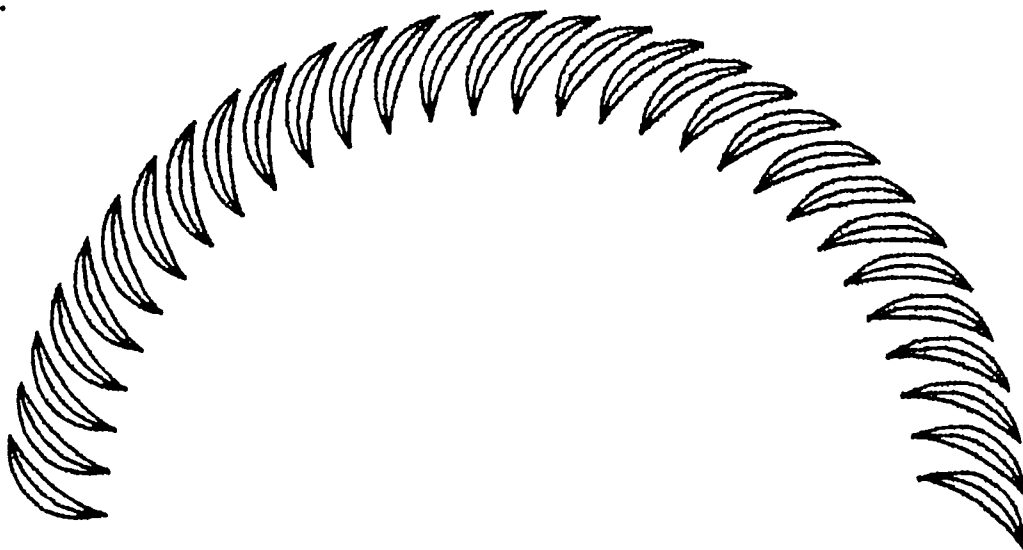


Figure B5. Schematic for Rotation of Axes.



$R_0 = 4$ $R_1 = 3.2$ No. Blades = 60

$\gamma = 9.1.72521902$ $\phi = 80.82738092$

Condition of Tangency is

$\sin \phi = \cos$

$\sin \phi = 0.159407755$ $\cos = 0.159409430$

chord = 0.983540343 chord test = 0.983540073

alpha = 18.34514098

radial solidity = 1.909859317

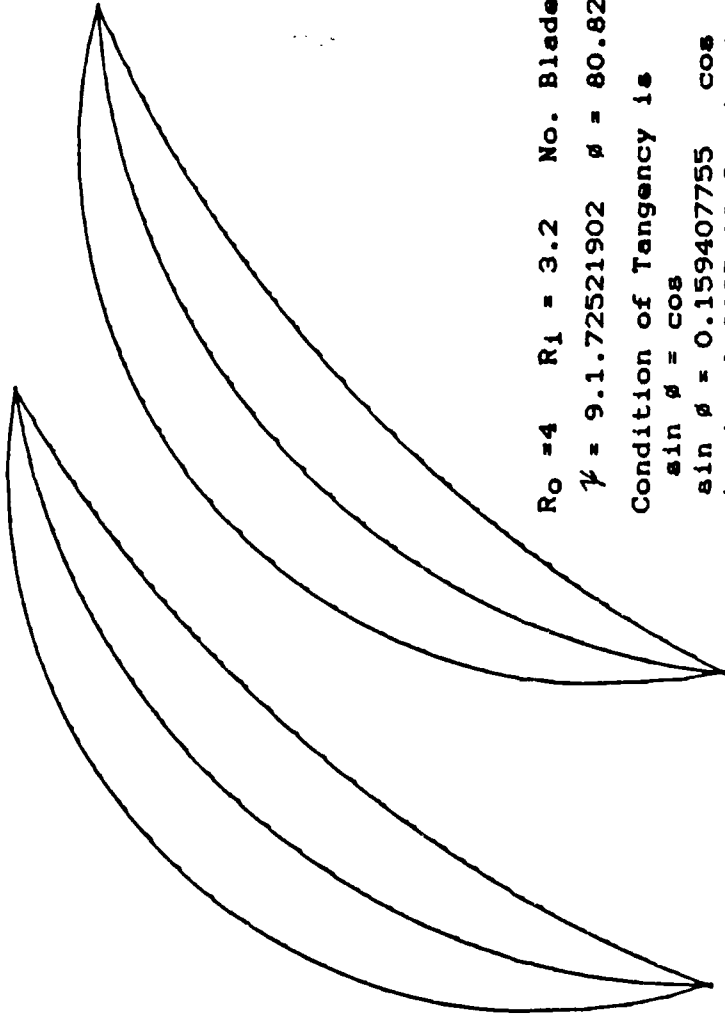
thickness to chord ratio = 0.194933797

radius of camber circle = 0.758551242

radius of suction circle = 0.575175292

radius of pressure circle = 1.462802226

Figure B6. Computer Generated Shapes
for a 60 Blade Design.



$R_0 = 4$ $R_1 = 3.2$ No. Blades = 60

$\psi = 9.1.72521902$ $\phi = 80.82738092$

Condition of Tangency is

$\sin \phi = \cos$

$\sin \phi = 0.159407755$ $\cos = 0.159409430$

chord = 0.983540343 chord test = 0.983540073

alpha = 18.34514098

radial solidity = 1.909859317

thickness to chord ratio = 0.194933797

radius of camber circle = 0.758551242

radius of suction circle = 0.575175292

radius of pressure circle = 1.462802226

Figure B7. Computer Generated Blade Passage
for a 60 Blade Design.

APPENDIX C

WEDGE-ARC BLADING DESIGN

C.1 METHOD

Because of the limitations seen in the outlet passage shapes which could be generated using purely double circular arc blades, symmetrical linear surface segments were added in an attempt to achieve a convergent nozzle at a shallow angle at the rim exit.

From the design using only double circular arcs it was found that by using the original camber line and the suction line to describe the blade, improved convergency at the exit was obtained (see figure C1). Removing the original pressure line would cause the flow to be at a small incidence angle at the inlet, but this was thought to be acceptable.

By allowing the flow to exit over a straight suction side from the exit of the passage, better control of the outlet flow angle was assured. The wedge arc geometry is shown in figure C2.

Referring to figure C2, the wedge arc blade shape was developed to have the following features, or constraints:

1. The pressure side is a circular arc.
2. The suction side between point H and I is a circular arc, between straight and symmetrical line segments.

3. A wedge angle (ϕ) is specified at the leading and trailing edges.
4. Equal leading edge and trailing edge thicknesses (δ) are specified.
5. The radius to the suction surface at the point of tangency to the straight segment, (point I) intersects the pressure surface of the adjacent blade at the trailing edge (point C'), or downstream of point C', depending on the value of the parameter (δ')

Referring to figure C2 and C3 the following relationships are obtained:

$$x_F = x_C - \delta' \cos \phi \quad C(1)$$

$$y_F = y_C + \delta' \sin \phi \quad C(2)$$

where δ' is the leading edge and trailing edge thickness. The value of δ' has been made dimensionless by dividing by R_0 . All other quantities have been made dimensionless in the procedures given in appendix B.

$$x_t = x_C - \delta/2 \cos \phi \quad C(3)$$

$$y_t = y_C + \delta/2 \sin \phi \quad C(4)$$

$$x_e = -\delta \quad C(5)$$

$$y_e = R_1 \quad C(6)$$

$$x_L = -\delta/2 \quad C(7)$$

$$y_L = R_1 \quad C(8)$$

The wedge angle, ϵ is specified. With ϵ known, the length of the straight section (l) from the exit can be found. For a symmetric blade, the length (l) is the same at the inlet and the exit. Referring to figure C2, C3 and C4

$$l = l'(1 - \epsilon) \quad \text{C(9)}$$

where $l = l'$ when the point I lies on the radius $C'D'$ (figure C4). The slope of the line $C'F$ (μ) is given by,

$$\mu = \text{arc tan} \left(\frac{y_F - y_{C'}}{x_F - x_{C'}} \right) \quad \text{C(10)}$$

The coordinates of C' are found by solving for the previous blade and rotating the coordinates. These values are placed in an array until needed. A straight line is drawn from the current blade to the previous blade as is defined as

$$C'F = \left([y_F - y_C]^2 + [x_F - x_{C'}]^2 \right)^{1/2} \quad \text{C(11)}$$

Referring to figure C3, the slope of FG is given by,

$$\Delta = [\alpha - \psi - \epsilon] \quad \text{C(12)}$$

A relationship of l' , $C'F$ and the line FG is given by,

$$\begin{aligned} l' &= C'F \cos C'FG \\ &= C'F \cos [\alpha - \psi - \epsilon + \mu] \quad \text{C(13)} \end{aligned}$$

From equation C(13) the coordinates of I and H are found,

$$x_I = x_F - l \cos [\alpha - \psi - \epsilon] \quad \text{C(14)}$$

$$y_I = y_F - l \sin (\alpha - \gamma - \epsilon) \quad C(15)$$

$$x_H = - [\delta + l \sin (\epsilon)] \quad C(16)$$

$$y_H = R_1/R_0 + l \cos (\epsilon) \quad C(17)$$

The centers of the suction side are given by either,

$$x_{D'} = x_H + R_z \cos (\epsilon) \quad C(18)$$

$$y_{D'} = y_H + R_z \sin (\epsilon) \quad C(19)$$

or,

$$x_{D'} = x_I + R_z \sin (\alpha - \gamma - \epsilon) \quad C(20)$$

$$y_{D'} = y_I - R_z \cos (\alpha - \gamma - \epsilon) \quad C(21)$$

From equations C(17), C(19) and C(11) R_z can be found

since

$$x_I - x_H = R_z (\cos (\epsilon) - \sin \Delta)$$

yielding,

$$R_z = \frac{x_I - x_H}{\cos (\epsilon) - \sin \Delta} \quad C(22)$$

To calculate the position of I for a given throat dimension (a') at the exit, further manipulation is required. Referring to figure C4, where "a" denotes the center of the exit throat,

$$x_a = x_{C'} + a' \sin \alpha \quad C(23)$$

and

$$y_a = y_{C'} - a' \cos \alpha \quad C(24)$$

From equations C(21), C(13) and C(15),

$$\begin{aligned} R_z &= \frac{(x_F - l \frac{\cos \Delta + \delta + l \sin (\epsilon)}{\cos (\epsilon) - \sin \Delta})}{\cos (\epsilon) - \sin \Delta} \\ &= \frac{x_F + \delta + l \frac{[\sin (\epsilon) - \cos \Delta]}{[\cos (\epsilon) - \sin \Delta]}}{\cos (\epsilon) - \sin \Delta} \quad C(25) \end{aligned}$$

Referring to figure C4

$$[R_z + a']^2 = [x_{D'} - x_a]^2 + [y_a - y_{D'}]^2 \quad C(26)$$

Using equation C(20) and C(21) the above equation becomes,

$$[R_z + a']^2 = [x_I - R_z \sin \Delta - x_a]^2 + [y_a - y_I - R_z \cos \Delta]^2$$

referring to equations C(14), and C(15),

$$[R_z + a']^2 = [x_F - l \cos \Delta + R_z \sin \Delta - x_a]^2 + [y_a - y_F + l \sin \Delta - R_z \cos \Delta]^2$$

which reduces to

$$\begin{aligned} 2R_z a' + a'^2 &= (x_F - x_a)^2 + (y_a - y_F)^2 + l^2 \quad C(27) \\ &+ 2l \cos \Delta (x_a - x_F) + 2l \sin \Delta (y_a - y_F) \\ &+ 2R_z \cos \Delta (y_a - y_F) + 2R_z \sin \Delta (x_F - x_a). \end{aligned}$$

Using equation C(25) the following results can be obtained

$$\begin{aligned} a'^2 &= (x_F - x_a)^2 + (y_a - y_F)^2 + l^2 + 2l \cos \Delta (x_a - x_F) \\ &+ 2l \sin \Delta (y_a - y_F) \\ &+ 2 \left(\frac{x_F + \delta + l[\sin(-\cos \Delta)]}{[\cos(-\sin \Delta)]} \right) \sin \Delta (x_F - x_a) \\ &+ 2 \left(\frac{x_F + \delta + l[\sin(-\cos \Delta)]}{[\cos(-\sin \Delta)]} \right) \cos \Delta (y_a - y_F) \\ &+ 2 \left(\frac{x_F + \delta + l[\sin(-\cos \Delta)]}{[\cos(-\sin \Delta)]} \right) a' \end{aligned}$$

$$[\cos(-\sin \Delta)] a'^2 = [\cos(-\sin \Delta)] * \quad C(28)$$

$$\begin{aligned} &\left((x_F - x_a)^2 + (y_a - y_F)^2 + l^2 \right. \\ &\quad \left. + 2l \cos \Delta (x_a - x_F) + 2l \sin \Delta (y_a - y_F) \right) \\ &+ 2 \frac{x_F + \delta + l[\sin(-\cos \Delta)]}{[\cos(-\sin \Delta)]} \sin \Delta (x_F - x_a) \\ &+ 2 \frac{x_F + \delta + l[\sin(-\cos \Delta)]}{[\cos(-\sin \Delta)]} \cos \Delta (y_a - y_F) \\ &+ 2 \frac{x_F + \delta + l[\sin(-\cos \Delta)]}{[\cos(-\sin \Delta)]} a' \end{aligned}$$

and on combining terms,

$$\begin{aligned}
 [\cos (\delta - \sin \Delta) a']^2 &= [\cos (\delta - \sin \Delta)] & C(29) \\
 &+ (2 [\cos (\delta - \sin \Delta)] \cos \Delta (x_a - x_F) \\
 &\quad + 2 [\cos (\delta - \sin \Delta)] \sin \Delta (y_a - y_F)) \ell \\
 &+ 2 x_F \sin \Delta (x_F - x_a) + 2 \delta \sin \Delta (x_F - x_a) \\
 &+ 2 [\cos (\delta - \sin \Delta)] \sin \Delta (x_F - x_a) \\
 &+ 2 x_F \cos \Delta (y_a - y_F) + 2 \delta \cos \Delta (y_a - y_F) \\
 &+ 2 [\cos (\delta - \sin \Delta)] \cos \Delta (y_a - y_F) \\
 &+ 2 x_F a' + 2 \delta a' + 2 a' [\cos (\delta - \sin \Delta)]
 \end{aligned}$$

$$\begin{aligned}
 [\cos (\delta - \sin \Delta) a']^2 &= [\cos (\delta - \sin \Delta)] \ell^2 & C(30) \\
 &+ (2 [\cos (\delta - \sin \Delta)] \cos \Delta (x_a - x_F) \\
 &\quad + 2 [\cos (\delta - \sin \Delta)] \sin \Delta (y_a - y_F) \\
 &\quad + 2 [\cos (\delta - \sin \Delta)] \sin \Delta (x_F - x_a) \\
 &\quad + 2 [\cos (\delta - \sin \Delta)] \cos \Delta (y_a - y_F) \\
 &\quad + 2 a' [\cos (\delta - \sin \Delta)]) \\
 &+ 2 x_F \sin \Delta (x_F - x_a) + 2 \delta \sin \Delta (x_F - x_a) \\
 &+ 2 x_F \cos \Delta (y_a - y_F) + 2 \delta \cos \Delta (y_a - y_F) \\
 &+ 2 x_F a' + 2 \delta a'
 \end{aligned}$$

The above equation is quadratic in the unknown ℓ , and a solution can be written explicitly. The value of ℓ can be found using equation C(9). The result is as follows,

If

$$B = (2 [\cos (\delta - \sin \Delta)] \cos \Delta (x_a - x_F) \quad C(31)$$

$$\begin{aligned}
& + 2 [\cos (\delta - \sin \Delta)] \sin \Delta (y_a - y_F) \\
& + 2 [\cos (\delta - \sin \Delta)] \sin \Delta (x_F - x_a) \\
& + 2 [\cos (\delta - \sin \Delta)] \cos \Delta (y_a - y_F) \\
& + 2 a' [\cos (\delta - \sin \Delta)] / l'^2 [\cos (\delta - \sin \Delta)]
\end{aligned}$$

$$\begin{aligned}
\text{Let } C = & 2 x_F \sin \Delta (x_F - x_a) + 2 \delta \sin \Delta (x_F - x_a) & C(32) \\
& + 2 x_F \cos \Delta (y_a - y_F) + 2 \delta \cos \Delta (y_a - y_F) \\
& + 2 x_F a' + 2 \delta a') / l'^2 [\cos (\delta - \sin \Delta)]
\end{aligned}$$

then our quadratic equation is,

$$0 = l'^2 [\cos (\delta - \sin \Delta)] (1 - (\delta'))^2 + 2B l'^2 [\cos (\delta - \sin \Delta)] + C(33)$$

$$(1 - (\delta')) + C l'^2 [\cos (\delta - \sin \Delta)] \quad C(34)$$

and is of the form,

$$0 = (1 - (\delta'))^2 + 2B(1 - (\delta')) + C \quad C(35)$$

so that

$$\begin{aligned}
(1 - (\delta')) & = -2B/2 \pm \frac{\sqrt{(2B)^2 - 4C}}{2} \\
& = -B \pm \sqrt{(B^2 - C)} \quad C(36)
\end{aligned}$$

The following possibilities occur:

1. If the term under the square root is negative then a solution does not exist.
2. If the term under the square root is positive, and the value of $(1 - (\delta'))$ is between 0 and 1 then a solution exists; the solution is

$$(1 - (\delta')) = -B + \sqrt{(B^2 - C)}$$

3. If the value of $(1 - (1))$ obtained in step (2) is outside the range of 0 to 1 then the solution is,

$$(1 - (1)) = -B - \sqrt{(B^2 - C)}$$

4. If the value of $(1 - (1))$ obtained in step (3) is outside the range of 0 to 1 then no solution exists.

Once (1) has been determined and all other values have been found, the design is complete and the blades can be drawn.

Referring to figure C2, to draw the radius on the leading edge the points

$$x = x_L + \delta/2 \cos \theta \quad C(37)$$

$$y = y_L - \delta/2 \sin \theta \quad C(38)$$

are plotted over the interval of θ between 0 and 180 degrees. The radius on the trailing edge is given by,

$$x = x_T - \delta/2 \cos \theta \quad C(39)$$

$$y = y_T + \delta/2 \sin \theta \quad C(40)$$

plotted over the interval of θ between θ and $\theta+180$.

To draw successive blades on the rotor the procedure is to rotate the axes after each blade is drawn. The procedure is described by equation B(55) and B(56).

C.2 COMPUTER PROGRAM "AWEDG"

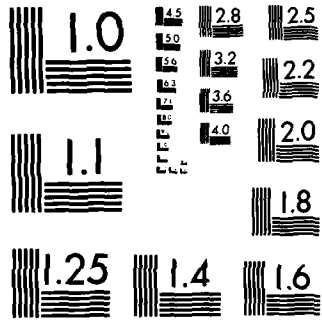
C.2.1 Description

The wedge arc blade design program, "AWEDG" calculates and draws wedge arc blading for an initially radial-outflow rotor. The difference between "AWEDG" and "ACIRC" is not only the specified input parameters; "AWEDG" calculates the straight section needed on the suction side to constrict the flow to a known dimension at the trailing edge tip of the adjacent blade. The program, for simplification, is divided into seven parts and each part will be described.

The first part (lines 1 to 460) contains the values of all specified parameters. On running, it also allows the user to specify the angles ψ and θ to determine early in the program what the value of α will be. If the user wishes to change the value of α he can do so. Chord length, camber radius and α are calculated in this section.

The second part (lines 470 to 640) prints some of the output parameters and calculates the center coordinates of the camber line.

In order to calculate the outlet passage size the preceding passage must be analyzed. The program does this in part three (line 650 to 800) by calculating the position of the trailing edge tip of the preceding pressure



MICROCOPY RESOLUTION TEST CHART
NATIONAL BUREAU OF STANDARDS-1963-A

line. Point C' on figure C3 is calculated by rotation of axes.

In part four (lines 810 to 1020) the position of points C, F, T, E, and L, shown in figure C3, are calculated.

Part five (beginning on line 1030) starts the plotting routine. The number of the blades requested to be drawn are specified. The pressure side radius is calculated and is drawn. Calculations for the straight line segments are performed (lines 1340 to 1570). Based on the determined value of the straight segment the coordinates of point I are derived (lines 1630 to 2090).

In part six the radius of the suction side is drawn. Plotting for the leading and trailing edge radius are also accomplished in part six.

Part seven (2100 to 2140) concludes the procedure by printing the value of the throat diameter, length of the straight line segment and radii of pressure and suction circle.

C.2.2 Required Inputs

The following inputs are required:

Outer radius

Inner radius

Total number of blades

angle γ

angle ϕ (must be consistent with ψ - see discussion)

Diameter of the circle at the passage exit

Leading edge and Trailing Edge thickness

Leading edge and Trailing Edge wedge angle

Number of blades requested to be drawn

C.2.3 Listed Outputs

The following quantities are output:

Outer radius

Inner radius

Number of blades

Angle ψ

Angle ϕ

Angle α

Radial solidity

Chord length

Thickness to chord ratio

Leading edge and trailing edge thickness

Leading edge and trailing edge wedge angle

Throat width at exit

Radius of the pressure surface

Radius of the suction surface

Length of the straight section on the suction side.

C.2.4 Program Listing

Listed here is the program "AWEDG" for the design of wedge shaped air blades. Table C2 identifies the symbols used in the program with the defined parameters. Figure C6 and C7 illustrates computer generated shapes for an outer radius of 4 inches, an inner radius of 3.2 inches and 60 blades. The value of ψ and θ are specified parameters to limit the efflux angle α to between 8 and 9 degrees.

```
10 REM*****AWEDG 1 AUGUST 1984*****
20 REM***PROGRAM TO CALCULATE & DRAW ARC BLADING***
30 REM***ARCS AND STRAIGHT BACKING FOR AN***
35 REM***INITIALLY OUTFLOW CASCADE*****
40 DEG
50 DIM G[100],H[100],U[100],V[100]
60 SCALE -1,1,-1,1
70 DISP "SET PLOTTER 7(X) BY 7(Y)-<CONT>";
80 STOP
90 REM*****
100 DISP "ENTER THE OUTER RADIUS";
110 INPUT R0
120 DISP "ENTER THE INNER RADIUS";
130 INPUT R1
140 R4=R1/R0
150 DISP "ENTER THE NUMBER OF BLADES";
160 INPUT Z0
170 L=0
180 S5=360/Z0
190 P1=3.141592654
200 S2=2*P1*R0/Z0
210 R9=(R0-R1)/S2
220 S1=(R0-R1)/S2
230 S0=S2/R0
240 R2=S0*S1
250 DISP "ENTER PSI-< BTWN LE & TE 0-360/Z";
260 INPUT S3
270 DISP "ENTER PHI-PRESSURE ANGLE/CAMBER";
280 INPUT T0
290 A0=90+S3-T0
300 PRINT "ALPHA IS DESIRED BWTN 8-9 DEGREES. THE VALUE"
```

```

310 PRINT "OF PSI&PHI CHOSEN WILL YIELD AN"
320 PRINT "ALPHA="A0"DEGREES"
330 PRINT "PSI="S3"AND PHI="T0
340 DISP "WISH TO CHANGE PSI&PHI Y=1,N=0";
350 INPUT O1
360 IF O1=1 THEN 250
370 DISP "ENTER THE LE & TE THICKNESS";
380 INPUT Q1
390 M0=Q1/R0
400 DISP "ENTER LE & TE WEDGE ANGLE";
410 INPUT M1
420 C1=R0*SIN(S3/SIN(T0/2)
430 C0=C1/R0
440 R3=C0/(2*SIN(T0/2))
450 R4=R1/R0
460 Q3=R3*R0
470 REM*****
480 REM*****PRINT STATEMENTS*****
490 PRINT "R0="R0"RI="R1"NO. BLADES="Z0
500 PRINT "PSI="S3
510 PRINT "PHI="T0
520 PRINT "CHORD="C1
530 PRINT "ALPHA="A0
540 PRINT "RADIAL SOLIDITY="R9
550 PRINT "LE & TE THICKNESS="Q1
560 PRINT "LE & TE WEDGE ANGLE="M1
570 DISP "ENTER THE THROAT LENGTH A=";
580 INPUT A5
590 REM*****END PRINT STATEMENTS*****
600 REM*****
610 REM****CENTERS CAN NOW BE DETERMINED****
620 X3=R3
630 Y3=R4
640 REM****DRAW BLADE SURFACES****
650 REM****FIRST CALCULATE COORDINATE OF C' ON BLADE NO. Z-1*
660 N9=16
670 N8=7
680 N1=Z0
690 I=1
700 FOR T4=0 TO T0 STEP T0/N9
710 X4=X3-(R3*COS(T4))
720 Y4=Y3+(R3*SIN(T4))
730 X9=X4+COS((N1-1)*S5)+(Y4*SIN((N1-1)*S5))
740 Y9=Y4+COS((N1-1)*S5)-(X4*SIN((N1-1)*S5))
750 PLOT X9,Y9
760 U(I)=X9
770 V(I)=Y9
780 I=I+1
790 NEXT T4
800 PEN

```



```

805 REM***F & C ON PRESSURE LINE***
810 REM***SECOND CALCULATED THE COORDINATES OF***
820 N0=1
830 I=1
840 FOR T4=0 TO T0 STEP T0/N9
850 X4=X3-(R3*COS(T4))
860 Y4=Y3+(R3*SIN(T4))
870 X9=X4*COS((N0-1)*S5)+(Y4*SIN((N0-1)*S5))
880 Y9=Y4*COS((N0-1)*S5)-(X4*SIN((N0-1)*S5))
890 G[I]=X9
900 H[I]=Y9
910 I=I+1
920 NEXT T4
930 M2=G[N9+1]
940 M3=M2-M0*COST0
950 M4=M2-(M0/2)*COST0
960 L2=H[N9+1]
970 L3=L2+M0*SINT0
980 L4=L2+(M0/2)*SINT0
990 M5=-M0
1000 M6=-(M0/2)
1010 L5=R1/R0
1020 L6=R1/R0
1030 REM*****PLOTTING SECTION*****
1040 DISP "INPUT THE NUMBER OF BLADES TO DRAW";
1050 INPUT N
1060 REM-----EDIT NEXT LINE FOR PLOT RESOLUTION-----
1070 N9=16
1080 FOR N0=1 TO N
1090 REM***FOR PRESSURE LINE***
1100 I=1
1110 FOR T4=0 TO T0 STEP T0/N9
1120 X4=X3-(R3*COS(T4))
1130 Y4=Y3+(R3*SIN(T4))
1140 X9=X4*COS((N0-1)*S5)+(Y4*SIN((N0-1)*S5))
1150 Y9=Y4*COS((N0-1)*S5)-(X4*SIN((N0-1)*S5))
1160 G[I]=X9
1170 H[I]=Y9
1180 I=I+1
1190 PLOT X9,Y9
1200 NEXT T4
1210 PEN
1220 REM***SUCTION SIDE LINE***
1230 REM***VALUE OF L SOLVED FOR WILL BE GENERATED***
1240 REM***TO GIVE THE DESIRED THROAT AT EXIT*****
1250 E1=L3-V[N9+1]
1260 E2=M3-U[N9+1]
1270 L0=ATN(-E1/E2)
1280 C3=SQR(E1^2+E2^2)

```

```

1290 D1=A0-S3-M1
1300 B9=C3*COB(A0-S3+L0-M1)
1310 REM***CALCULATION OF BLADE SUCTION SURFACE***
1315 REM***FOR A GIVEN THROAT SIZE AT EXIT***
1320 REM***A4 IS THE RADIUS AT THE THROAT A5/2***
1330 A4=A5/(2*R0)
1340 X6=V(N9+1)+A4*SINA0
1350 Y6=V(N9+1)-A4*COB A0
1360 Z5=(SIND1*(Y6-L3)+COSD1*(X6-M3))*(COSM1-SIND1)
1370 Z6=(SIND1*(M3-X6)+COSD1*(Y6-L3)-A4)*(SINM1-COSD1)
1380 Q1=(Z5+Z6)/(C3*(COSM1-SIND1))
1390 Z7=(2*(M3+M0)*(SIND1*(M3-X6)+COSD1*(Y6-L3)-A4))
1400 Z8=((M3-X6)2+(Y6-L3)2-A42)*(COSM1-SIND1)
1410 Q2=(Z7+Z8)/(C32*(COSM1-SIND1))
1420 Q3=Q12-Q2
1430 IF Q3<0 THEN 1560
1440 Q4=-Q1+SQB(Q3)
1450 IF 0<Q4<1 THEN 1470
1460 IF Q4<0 OR Q4>1 THEN 1500
1470 REM***FIRST SOLUTION FOR E=(1-Q4)***
1480 T9=1-Q4
1490 GOTO 1550
1500 Q5=-Q1-SQB(Q3)
1510 IF 0<Q5<1 THEN 1530
1520 IF Q5<0 OR Q5>1 THEN 1560
1530 REM***SECOND SOLUTION FOR E=(1-Q5)***
1540 T9=1-Q5
1550 GOTO 1570
1560 PRINT "NO SOLUTION EXISTS"
1570 B8=B9*(1-T9)
1580 M7=M3-B8*COSD1
1590 L7=L3-B8*SIND1
1600 M8=-(M0+B8*SINM1)
1610 L8=R1/R0+B8*COSM1
1620 REM***RADIUS OF SUCTION SIDE***
1630 R7=(M7-M8)/(COSM1-SIND1)
1640 REM***CENTERS OF SUCTION RADIUS***
1650 X5=M8+R7*COSM1
1660 Y5=L8+R7*SINM1
1670 REM***PLOT ROUTINE TO DRAW SUCTION SIDE***
1680 REM***PLOT RADIUS ON LE TIP***
1690 FOR T4=0 TO 180 STEP 180/N8
1700 X4=M6+(M0/2)*COB T4
1710 Y4=L6-(M0/2)*SIN T4
1720 X9=X4*COB((N0-1)*S5)+(Y4*SIN((N0-1)*S5))
1730 Y9=Y4*COB((N0-1)*S5)-(X4*SIN((N0-1)*S5))
1740 PLOT X9,Y9
1750 NEXT T4

```

```

1760 X4=M8
1770 Y4=L8
1780 X9=X4*COS((N0-1)*S5)+(Y4*SIN((N0-1)*S5))
1790 Y9=Y4*COS((N0-1)*S5)-(X4*SIN((N0-1)*S5))
1800 PLOT X9,Y9
1810 REM***PLOT SUCTION RADIUS***
1820 I1=-M1
1830 I2=2*M1+T0
1840 I3=(I2-I1)/N9
1850 FOR T4=I1 TO I2 STEP I3
1860 X4=X5-R7*COST4
1870 Y4=Y5+R7*SINT4
1880 X9=X4*COS((N0-1)*S5)+(Y4*SIN((N0-1)*S5))
1890 Y9=Y4*COS((N0-1)*S5)-(X4*SIN((N0-1)*S5))
1900 PLOT X9,Y9
1910 NEXT T4
1920 X4=M3
1930 Y4=L3
1940 X9=X4*COS((N0-1)*S5)+(Y4*SIN((N0-1)*S5))
1950 Y9=Y4*COS((N0-1)*S5)-(X4*SIN((N0-1)*S5))
1960 PLOT X9,Y9
1970 REM***PLOT RADIUS ON THE TE TIP***
1980 I1=T0
1990 I2=T0+180
2000 I3=(I2-I1)/N8
2010 FOR T4=I1 TO I2 STEP I3
2020 X4=M4-(M0/2)*COST4
2030 Y4=L4+(M0/2)*SINT4
2040 X9=X4*COS((N0-1)*S5)+(Y4*SIN((N0-1)*S5))
2050 Y9=Y4*COS((N0-1)*S5)-(X4*SIN((N0-1)*S5))
2060 PLOT X9,Y9
2070 NEXT T4
2080 PEN
2090 NEXT N0
2100 PRINT "R*="A5
2110 PRINT "L="B8
2120 PRINT "RADIUS OF PRESSURE CIRCLE ="03
2130 PRINT "RADIUS OF SUCTION CIRCLE="(R7*R0)
2140 END

```

TABLE C1. List of Computer and Text Symbols
for Wedge-Arc Blade.

"AWEDG"	TEXT	IDENTIFICATION
A0	α	efflux angle
A4	-	throat dimension (radius of outlet circle)
A5	$2*a'$	throat diameter (diameter of exit circle)
B8	l	length of straight section
B9	l'	length of straight section to be tangent to outlet circle
C0	c''	c/R_0 dimensionless, chord length
C1	c	chord length
D1		constant angle
E1	-	constant value
E2	-	constant value
G[I]	-	array for current pressure side x coordinates
H[I]	-	array for current pressure side y coordinates
I	-	counter
I1	-	Interval variable
I2	-	Interval variable
I3	-	Interval variable

TABLE C1. List of Computer and Text Symbols for Wedge-Arc Blade (con't).

"AWEDGE"	TEXT	IDENTIFICATION
L2	yc	final value on present pressure line, y coordinate
L3	yF	final value on present pressure line plus blade thickness, y coordinate
L4	yt	center point of trailing edge, y coordinate
L5	YE	Leading edge initial suction side, y coordinate
L6	YI	point of tangency for suction side, y coordinate
L7	YI	point of tangency for suction side, y coordinate
L8	YH	initial point for suction side curve, y coordinate
M0	δ	Leading and trailing edge thickness
M1	ϵ	Leading and trailing edge wedge angle
M2	xc	final value on present pressure line, x coordinate
M3	xF	final value on present pressure line plus blade thickness, x coordinate
M4	xt	center point of trailing edge, x coordinate
M5	xE	Leading edge initial suction side, x coordinate

TABLE C1. List of Computer and Text Symbols for Wedge-Arc Blades (con't).

"AWEDGE"	TEXT	IDENTIFICATION
M6	x _L	center point of leading edge
M7	x _I	point of tangency for suction side, x coordinate
M8	x _H	initial point for suction side curve, x coordinate
N	N	Number of blades to draw
NO	-	Number of blades to draw for loop
N9	-	Number of points for interval of arc
O1	-	Equals 1 to change ψ and θ , 0 for no
O3	R _C	output print of R _C
O4	R _S	output print of R _S
P1	π	π
Q1	-	constant
Q2	-	constant
Q3	-	constant, value under square root term for solving for ξ
Q4	-	same as Q3
Q5	-	same as Q3
RO	R _O	outer radius

TABLE C1. List of Computer and Text Symbols for Wedge-Arc Blades (con't).

"AWEDGE"	TEXT	IDENTIFICATION
R1	R_i	inner radius
R2	ρ	radial chord, $(R_0 - R_i)/R_0$
R3	R_c/R_0	camber line radius, dimensionless
R4	R_i/R_0	inner radius, dimensionless
R6	R_p/R_0	pressure radius, dimensionless
S0	s	peripheral spacing, $2\pi R_0/Z$
S1	σ_r	radial solidity
S2	s/R_0	dimensionless peripheral spacing
S3	γ	blade curvature with respect to center of rotor
S5	γ_s	spacing angle, $360/Z$
T0	θ	camber angle
T4	-	loop parameter to draw arcs
T9	-	value of $1-(\prime$
X2	x_{dp}	pressure surface center, x coordinate
X3	x_d	camber line center, x coordinate
X4	-	variable for x values in continuous loop
X9	-	variable for x values in rotational loop

TABLE C1. List of Computer and Text Symbols for Wedge-Arc Blades (con't).

"AWEDGE"	TEXT	IDENTIFICATION
Y2	ydp	pressure center y coordinate
Y3	yd	camber center y coordinate
Y4	-	variable for y values in continuous loop
Y9	-	variables for y values in rotational loop
Z0	Z	number of blades

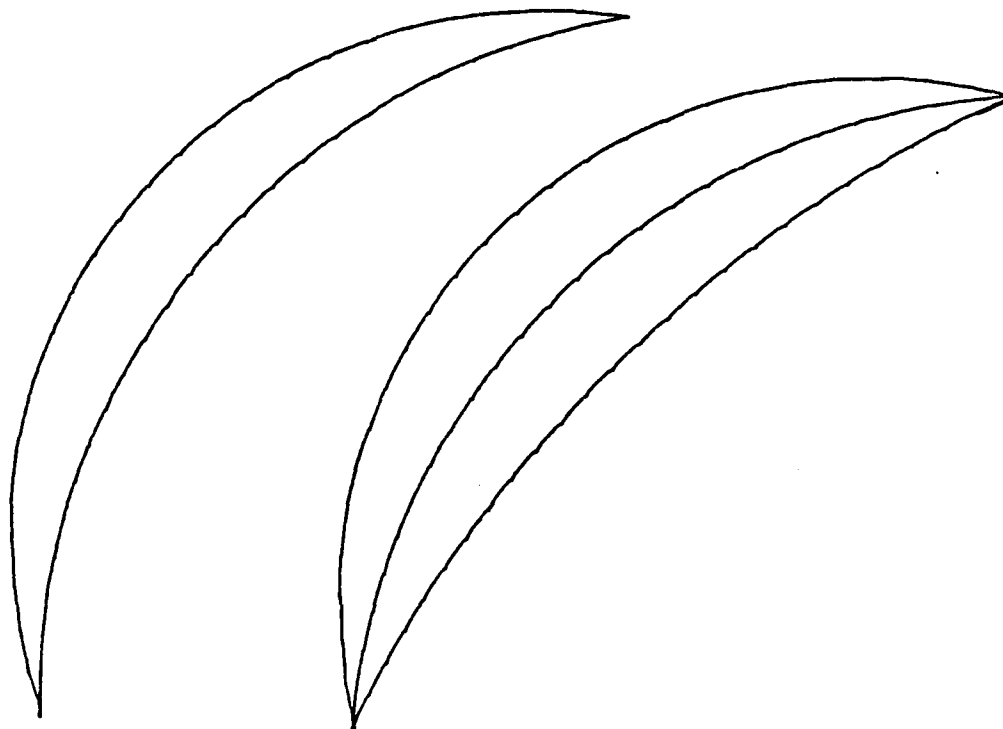


Figure C1. Relaxed Double Circular Arc Passage
with Pressure Line Removed.

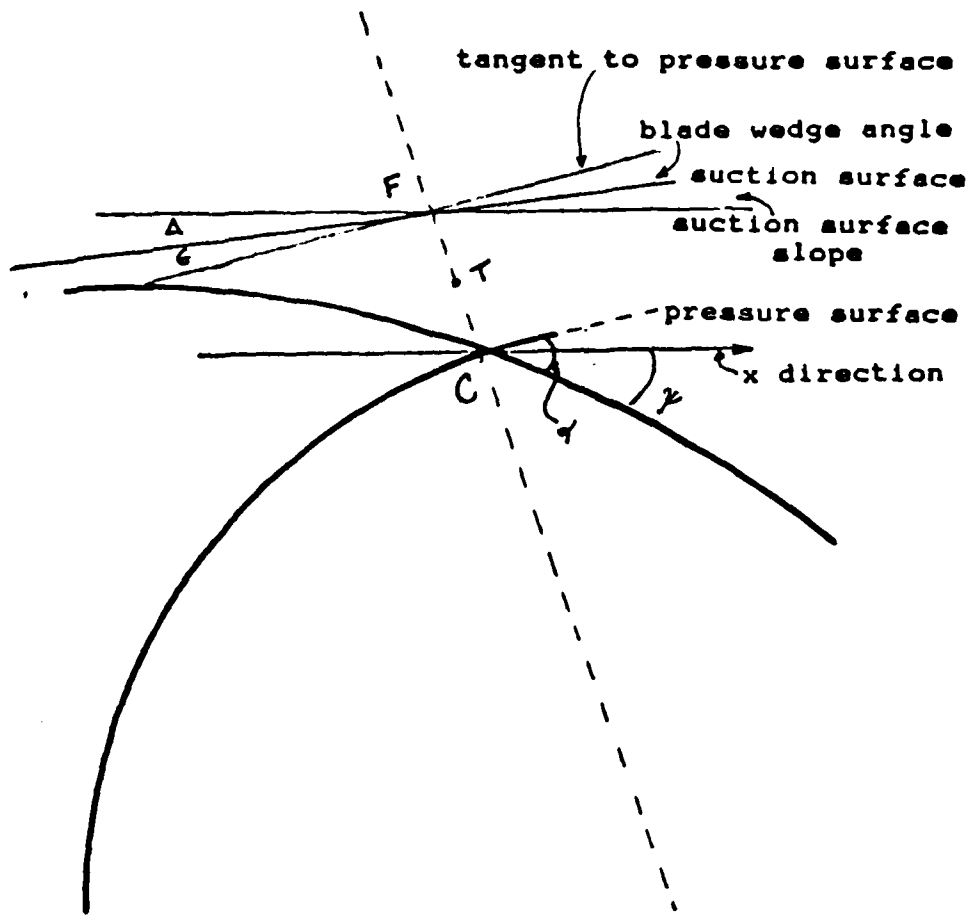


Figure C3. Enlarged View of Trailing Edge.

$R_o = 4$ $R_i = 3.2$ No. of Blades = 60
 $\psi = 9.17$ $\phi = 90.68$
chord = 0.896198294
alpha = 8.49
radial solidity = 1.909859317
L.E. & T.E. thickness = 0.02
L.E. & T.E. wedge angle = 5
 $A^* = 0.05225$
 $L = 0.037306915$
radius of pressure circle = 0.629980625
radius of suction circle = 0.476827358

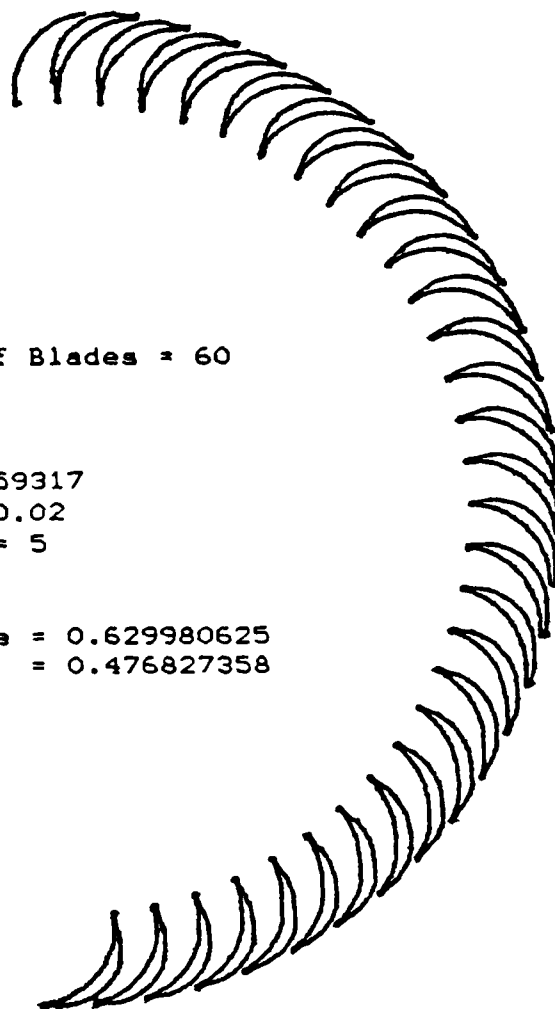
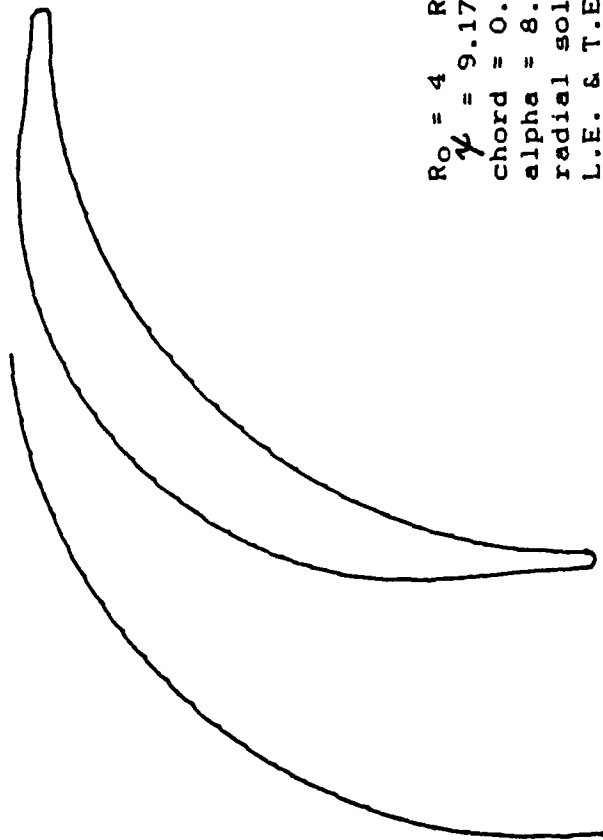


Figure C5. Computer Generated Shapes for a Cascade of Wedge Arc Shaped Blades with 60 Blades.



$R_o = 4$ $R_i = 3.2$ No. of Blades = 60
 $\psi = 9.17$ $\phi = 90.68$
chord = 0.896198294
alpha = 8.49
radial solidity = 1.909859317
L.E. & T.E. thickness = 0.02
L.E. & T.E. wedge angle = 5
A* = 0.05225
L = 0.037306915
radius of pressure circle = 0.629980625
radius of suction circle = 0.476827358

Figure C6. Computer Generated Blade Passage
for Wedge Arc Shaped Blade.

LIST OF REFERENCES

1. Monks, S. A., Preliminary Assessment of a Rotary Detonative Engine Concept, M.S. Thesis, Naval Postgraduate School, Monterey, California, 1983.
2. Erwin, J. R., Development and Use of a Centrifugal Test Device, Naval Postgraduate School Turbopropulsion Laboratory Technical Proposal, 81-006, 1981.
3. Vidos, P., Flow Generation in a Novel Centrifugal Diffuser Test Device, M.S. Thesis, Naval Postgraduate School, Monterey, California, 1983.
4. Feiereisen, W. J., An Experimental Investigation of Incompressible Flow Without Swirl in R-Radial Diffusers, Ph.D Thesis, Purdue University, West Lafayette, Indiana 1971.
5. Vavra, M. H., Axial Turbine Design Data, Naval Postgraduate School Turbopropulsion Laboratory, Report 1174VA1, Nov. 1974
6. Demo Jr., W. J., Cascade Wind Tunnel for Transonic Compressor Blading Studies, M.S. Thesis, Naval Postgraduate School, Monterey, California, 1978.
7. Erwin, J. R., Notes on Centrifugal Diffuser Test Device, Naval Postgraduate School Turbopropulsion Laboratory (unpublished).
8. NASA Lewis Research Center Technical Note, NASA TN-D-4421, Analytical Investigation of Supersonic Turbomachinery Blading, I. Computer Program for Blading Design, by Goldman, L. J. and Scullin, V. J., March 1968.
9. NASA Lewis Research Center Technical Memo, NASA TM-X-2342, Computer Program for Design of Two Dimensional Sharp-Edge-Throat Supersonic Nozzle with Boundary Layer Correction, by Goldman, L. J. and Vanco, M. R., August 1971.
10. Horlock, J. H., Axial Flow Turbine, Fluid Mechanics and Thermodynamics, Butterworth and Co., 1966
11. NASA Scientific and Technical Publication, SP-290, Volume 3, Turbine Design and Application.

12. Technical Advances in Gas Turbine Design, The Institute of Mechanical Engineers Proceedings, Volume 183, Part 3N, 1968-1969.
13. Naval Postgraduate School, Contractor Report, NPS67-83-02CR, A Fortran Program for Solving Two Dimensional Euler Equations with Godunov Methods-User's, by Eidelman, S.

BIBLIOGRAPHY

1. Adamson Jr., J. C., and Platzer, M. F., Transonic Flow Problems in Turbomachinery, Hemisphere Publishing Co., 1977.
2. American Society of Mechanical Engineers, Symposium on Unsteady Flow, Washington, D. C., 1968
3. Dzung, L. S., Flow Research on Blading, Proceedings of the Symposium on Flow Research on Blading, Brown, Boveri, and Co. Limited Baden Switzerland, 1960.
4. Faulders, C. R., An Aerodynamic Investigation of Vane Diffusers for Centrifugal Compressors, Ph.D Thesis, Massachusetts Institute of Technology, Boston, Massachusetts 1954.
5. Johnsen, I. A., Aerodynamic Design of Axial-Flow Compressor, Lewis Research Center, 1956.
6. Logan Jr., E., Turbomachinery, Basic Theory and Applications, Marcel Dekker, Inc., 1981.
7. Markov, N. M., Calculation of the Aerodynamic Characteristics of Turbine Blading, North American Aviation Inc, 1958.
8. Moses, H. L., Turbomachinery, Supplementary Notes, Naval Postgraduate School, 1983.
9. Streeter, V. L., and Wylie, B. E., Fluid Mechanics, McGraw Hill, 1979
10. Vincent, E. T., The Theory and Design of Gas Turbines and Jet Engines, McGraw Hill, 1950.

INITIAL DISTRIBUTION LIST

	No. Copies
1. Defense Technical Information Center Cameron Station Alexandria, Virginia 22314	2
2. Library, Code 0142 Naval Postgraduate School Monterey, California 93943	2
3. Department Chairman, Code 69Mx Department of Mechanical Engineering Naval Postgraduate School Monterey, California 93943	1
4. Department Chairman, Code 67 Department of Aeronautics Naval Postgraduate School Monterey, California 93943	1
5. Dr. R. P. Shreeve, Code 67Sf Department of Aeronautics Naval Postgraduate School Monterey, California 93943	1
6. Professor R. H. Nunn, Code 69Nn Department of Mechanical Engineering Naval Postgraduate School Monterey, California 93943	1
7. U.S. Army Air Mobility R&D Laboratory (Attn: L. Schumann, MS. 5-9) NASA Lewis Research Center 21000 Brookpark Road Cleveland, Ohio	1
8. Turbopropulsion Laboratory Code 67 Naval Postgraduate School Monterey, California 93943	5
9. LT Pamela E. Thrower-LeSesne 1711 Tipton Drive Crofton, Maryland 21114	3

END

FILMED

7-85

DTIC